Investigating the influence of stratospheric ozone trends on Southern Hemisphere hydrological climate change

Ariaan Purich

Master of Science

Supervised by Professor Seok-Woo Son and Professor Jacques Derome

Department of Atmospheric and Oceanic Sciences

McGill University

Montréal, Québec

25 July 2011

A thesis submitted to McGill University in partial fulfillment of the requirements of the degree of Master of Science

Acknowledgements

I would like to acknowledge all the people who have contributed to this research. First and foremost I acknowledge the contributions of both my supervisors, Professor Seok-Woo Son and Professor Jacques Derome. Their support and guidance throughout this project has been invaluable and greatly appreciated. I also thank Professor Parisa Ariya for her helpful review comments, Neil Tandon for his coding assistance, Patrick Martineau for providing zonally averaged reanalysis data and Melissa Gervais for translating my abstract into French. Throughout my Master of Science I have been supported financially by the Stephen and Anastasia Mysak Graduate Fellowship, for which I am very grateful. I also acknowledge financial assistance from a Principal's Graduate Fellowship, a Provost's Graduate Fellowship, and to enable me to attend the IUGG 2011 conference in Melbourne, a GEC3 Travel Grant and an IAMAS Conference Grant. Finally I would like to acknowledge my family and friends, with particular mention to my parents and Vaughn, for their ongoing support in all of my pursuits.

Abstract

Changes in stratospheric ozone have previously been linked to Southern Hemisphere (SH) circulation changes. This study examines output from coupled climate models participating in the Climate Model Intercomparison Project 3 (CMIP3) for trends in precipitation and evaporation in the 20^{th} and 21^{st} centuries to assess whether stratospheric ozone influences the hydrological cycle and extreme precipitation in the SH extratropics, particularly during austral summer. Nineteen models are used, of which 10 incorporated ozone depletion (recovery) in the 20^{th} (21^{st}) century, whilst nine simply prescribed climatological ozone in both past and future climates. Trends in seasonal-mean precipitation are found to dominate overall changes in precipitation minus evaporation. For the 20^{th} century, models with ozone depletion show a significant increase (decrease) in summer precipitation in high latitudes (mid-latitudes) compared to models without ozone depletion. In contrast, for the 21^{st} century, models without ozone recovery show significantly larger changes in summer precipitation in these regions compared to models with ozone recovery. No significant differences, however, are found in the two sets of models during austral winter when stratospheric ozone is inactive. These results suggest that Antarctic ozone depletion and recovery significantly modulates hydrological climate change in the SH extratropics, in agreement with findings of previous studies. It is further found that stratospheric ozone primarily affects the frequency of light precipitation events (1–10 mm day^{-1}), indicating that an increase in mean precipitation over the Southern Ocean corresponds to an increase in the number of light precipitation days rather than extreme events. Implications of this finding to the SH surface climate and Southern Ocean circulation changes are discussed.

Résumé

Les changements de concentration d'ozone stratosphérique ont été déjà reliés aux changements de la circulation dans l'hémisphère sud (HS). Ce travail examine les tendances dans la précipitation et l'évaporation pendant les $20^{ième}$ et $21^{ième}$ siècles, dans des simulations produites par des modèles climatique couplés qui participent au Climate Model Intercomparison Project 3 (CMIP3). Le but est de déterminer si l'ozone stratosphérique influence le cycle hydrologique et la précipitation extrême aux latitudes extra-tropicales de l'HS, pendant l'été austral en particulier. Dix-neuf modèles sont utilisés, où 10 d'entre eux incorporent l'épuisement (le rétablissement) d'ozone au $20^{ième}$ ($21^{ième}$) siècle et les neuf autres prescrivent simplement l'ozone climatologique (du $20^{ième}$ siècle) pendant le passé et le futur. Les tendances des moyennes saisonnières de précipitation dominent les changements de l'évaporation moins la précipitation, alors c'est cette variable qui est examinée plus en détail. Pour le $20^{ième}$ siècle, il y a une augmentation (diminution) de précipitation significative en été aux latitudes subarctique (latitudes moyennes) dans les modèles avec l'épuisement d'ozone comparé à ceux avec l'ozone climatologique. En contraste, pour le $21^{ième}$ siècle, les changements de précipitation sont considérablement plus grands dans les modèles sans le rétablissement d'ozone que dans les modèles avec le rétablissement d'ozone. Pour l'hiver austral, quand l'ozone est inactif, il n'y a pas de différences entre les deux groupes de modèles. Ces résultats suggèrent que la diminution et rétablissement d'ozone dans l'Antarctique a des implications considérables pour le changement de climat hydrologique dans l'HS hors tropique, une conclusion atteinte dans d'autres travaux. En plus, on trouve que l'ozone stratosphérique affecte principalement la fréquence des évènements de précipitation légère (1–10 mm jour^{-1}), ce qui indique qu'une augmentation de la précipitation moyenne correspond à une augmentation du nombre de jours de

précipitation légère, plutôt que d'évènements extrêmes. Les implications de ces conclusions pour le climat à la surface ainsi que pour les changements de circulation dans l'océan de l'HS sont discutés.

Table of Contents

List of Tables

List of Figures

Chapter 1
Introduction

Southern Hemisphere (SH) climate changes over the last century have been extensively documented. They include a shift in atmospheric mass from high to mid-latitudes, an increase in the westerly wind speeds over the Southern Ocean, a poleward shift in storm tracks, surface cooling of the Antarctic continent and warming of the Antarctic peninsula, Argentina, Tasmania and southern New Zealand, an increase in the length of the sea ice season over much of eastern Antarctica, a retreat of ice shelves over the Antarctic peninsula, anomalously dry conditions over southern South America, New Zealand and Tasmania due to a poleward shift in storm tracks, and anomalously wet conditions over much of Australia and South Africa (Thompson and Solomon 2002; Marshall 2003; Gillett and Thompson 2003; Shindell and Schmidt 2004; Gillett et al. 2006). In the ocean, amongst other changes, a freshening and warming of the Southern Ocean has also been observed (Wong et al. 1999; Gille 2002, 2003; Boyer et al. 2005; Levitus et al. 2005; Böning et al. 2008; Forster et al. 2010).

Many of these changes have been attributed to anthropogenic emissions of greenhouse gases. However, it is known that increasing greenhouse gases cannot account for all changes, especially during austral summer. Those changes that cannot be explained by changes in greenhouse gas concentrations have been attributed to the stratospheric ozone depletion in the Antarctic region during the latter part of the 20^{th} century as a result of anthropogenic emissions of ozone depleting substances (ODSs) (Gillett and Thompson 2003; Shindell and Schmidt 2004; Arblaster and Meehl 2006; Karpechko et al. 2008;

Perlwitz et al. 2008; Son et al. 2008, 2009, 2010). Through tropospheric coupling, stratospheric ozone depletion enhances the SH circulation changes associated with greenhouse gas forcing. Previous studies investigating the influence of stratospheric ozone on the SH troposphere have predominantly focussed on changes in atmospheric circulation, surface temperature and pressure. To date there have not been many studies examining the impact of stratospheric ozone on SH hydrology. Thus the purpose of this research is to investigate the influence of stratospheric ozone changes on SH precipitation, evaporation and extreme precipitation events.

1.1 Background

The effect of stratospheric ozone depletion in the 20^{th} century has been linked to SH climate changes. This includes a rising extratropical tropopause, a poleward intensification of the extratropical eddy-driven westerly jet, a poleward shift in storm tracks and a poleward expansion of the Hadley cell (Arblaster and Meehl 2006; Seidel et al. 2008; Son et al. 2009, 2010). The poleward shift in storm tracks is predominantly the focus of hydrology-related trends research: with storm tracks moving poleward a dipole trend in precipitation is expected, with an increasing trend in precipitation on the poleward side of storm tracks (where the storm tracks are moving to) and a decreasing trend in precipitation on the equatorward side of storm tracks (where the storm tracks are moving from). Son et al. (2009) conducted a multimodel study using output from 20 models participating in the Climate Model Intercomparison Project 3 (CMIP3). By grouping models into those that prescribed ozone depletion in the 20^{th} century and those that did not, they found well defined dipole trends in the austral summer precipitation in the models with prescribed ozone depletion. Although they found qualititatively similar trends in the models with climatological ozone, these trends were much weaker. Thus Son et al. (2009) concluded that the stratospheric

ozone decline in the 20^{th} century likely caused changes in SH precipitation during summer.

In the 20^{th} century, increasing greenhouse gases and stratospheric ozone depletion have influenced the SH circulation in similar ways. For example, both forcings enhance precipitation in the SH high latitudes during austral summer. In the 21^{st} century atmospheric concentrations of greenhouse gases are expected to continue increasing and continue forcing SH circulation changes in the same direction as in the 20^{th} century. Stratospheric ozone, however, is expected to recover as a result of the implementation of the Montreal Protocol (Solomon et al. 2007; Austin et al. 2010; Forster et al. 2010) and thus the direction of SH circulation changes forced by stratospheric ozone is expected to reverse. Therefore, in the 21^{st} century SH climate change trends during austral summer may be weakened or even reversed relative to trends in the 20^{th} century depending on the relative intensity of greenhouse gas forcing and stratospheric ozone forcing. To aid predictions of 21^{st} century SH climate it is important to understand the relative importance of these two forcings.

1.2 Stratospheric ozone and climate change

Ozone-induced circulation changes have been examined in the context of the Southern Annular Mode (SAM) and westerly jet in the SH extratropics. A brief summary of the literature is provided here: the reader is referred to Chapter 2 for further details.

A negative trend in globally averaged total column ozone (TCO) was observed from 1980 to the mid-1990s, however recently this trend appears to have plateaued and a reduction in ODS loading appears to have occurred as a result of the implementation of the Montreal Protocol (Solomon et al. 2007; Forster et al. 2010). Since changes have been observed (1980), the largest ozone changes have occurred during late winter and spring

over Antarctica (Solomon et al. 2007). It is generally accepted that ozone recovery in the future will take a much longer time than ozone depletion in the past. Antarctic recovery to 1980 levels is predicted around the mid-21^{st} century, although it could occur as late as between 2060 and 2070 (Austin et al. 2010).

Stratospheric ozone loss in the Antarctic lower stratosphere induces a stratospheric cold anomaly, which is largest during November (Karpechko et al. 2008). The temperature anomaly in the polar stratosphere results in an increase in the stratospheric westerly polar vortex (Gillett and Thompson 2003). Changes in stratospheric winds can couple to the troposphere during late spring/early summer and during autumn (Thompson and Solomon 2002). Thus the maximum stratospheric temperature anomaly coincides with a time when the changes in the stratospheric polar vortex are coupled to the troposphere, invoking a change in the tropospheric SAM. The SAM is the dominant mode of atmospheric variability in the extratropical SH (Thompson and Wallace 2000; Marshall 2003). Pronounced tropospheric trends towards the positive phase of the SAM index have been observed during austral summer (Thompson and Solomon 2002; Marshall 2003).

This trend implies that the mean surface pressure in high latitudes is decreasing and the mean surface pressure in mid-latitudes is increasing relative to one another, inducing an intensification and poleward shift in the extratropical eddy-driven westerly jet. This trend is consistent with circulation changes associated with both a decrease in stratospheric ozone and an increase in the concentrations of atmospheric greenhouse gases (Arblaster and Meehl 2006), although the former is important only in late spring and summer whereas the latter occurs year-round (Perlwitz et al. 2008). It has been found that 20^{th} century climate simulations with increasing greenhouse gases reveal trends in the SAM index of the same

sign but considerably weaker magnitude than observations, indicating that ozone depletion has had an important influence on the tropospheric SAM trends (Gillett and Thompson 2003). Shindell and Schmidt (2004) and Arblaster and Meehl (2006) further showed that ozone depletion was the dominant contributor to observed changes in the mid-troposhere in summer while both greenhouse gas and stratospheric ozone forcing played a comparable role at the surface (Karpechko et al. 2008). Perlwitz et al. (2008) and Son et al. (2008) note that the scientific consensus finds the Antarctic ozone hole to be the biggest contributor to the observed tropospheric circulation changes during summer, but has a negligible role during other seasons.

A number of model studies have been undertaken to investigate SAM variability and trends in past and future climates, as well as the relative importance of ozone forcing and greenhouse gas forcing on these changes. However, the impact of trends in stratospheric ozone on the SH hydrological cycle still remains to be determined.

1.3 Study objectives

The purpose of this research is to investigate, by extending the research undertaken by Son et al. (2009), the influence of stratospheric ozone changes on SH hydrological changes. Analysis of both monthly-mean and daily-mean precipitation and evaporation data is undertaken using output from the CMIP3 database. Since trends in precipitation are found to dominate changes in the precipitation minus evaporation (P–E) balance during austral summer, they are examined in further detail to understand how stratospheric ozone affects SH hydrology. In particular, daily-mean precipitation data are analysed for trends in the frequencies and accumulations of different precipitation intensities (0.1–1 mm day^{-1}, 1–10 mm day^{-1} and >10 mm day^{-1}) and in a number of extreme precipitation indices (simple

precipitation index, sum of precipitation on days exceeding the 95^{th} and 99^{th} percentiles, maximum one-day precipitation and maximum five-day consecutive precipitation). The findings of this study are related to predictions of extreme precipitation in a warming climate. They are also applied to a discussion of the observed 20^{th} century changes in Southern Ocean characteristics (freshening and warming) and to speculate about changes in the 21^{st} century.

1.4 Document overview

This thesis begins with a discussion of the literature relevant to the study objectives in Chapter 2, including changes in stratospheric ozone concentration, the influence stratospheric ozone changes have on tropospheric climate and why changes in precipitation patterns are important. Following the literature review, the methodology is presented in Chapter 3, describing in detail the multimodel analysis undertaken and the statistical methods used to compare results. The results obtained are presented and discussed in Chapter 4. Chapter 5 provides a summary of the findings and a discussion of the significance of these findings to the Southern Ocean, along with recommendations for future work.

Chapter 2
Literature review

2.1 Climate change

Earth's climate is a constantly changing system on all time scales. The unprecedented environmental concern of our time is largely driven by anthropogenic-induced climate change: human activities are changing the global climate at such a rate that other systems cannot keep up.

Changes in the atmospheric concentrations of greenhouse gases and aerosols alter the energy balance of the climate system. Atmospheric levels of carbon dioxide, methane and nitrous oxide have increased markedly as a result of human activities since ∼1750, primarily due to fossil fuel use, land use change and agriculture. As a result of anthropogenic emissions of greenhouse gases, "warming of the climate system is unequivocal," (Solomon et al. 2007). Solomon et al. (2007) state that, "most of the observed increase in global average temperatures since the mid-20^{th} century is very likely due to the observed increase in anthropogenic greenhouse gas concentrations." Increased concentrations of greenhouse gases warm the global tropospheric climate and cause changes in other climate characteristics such as amplified temperature extremes, changed wind patterns, ocean warming, changed precipitation patterns and stratospheric cooling (Solomon et al. 2007).

Emission of ODSs such as chlorine- and bromine-containing substances in the latter part of the 20^{th} century has also contributed to climate change in both the stratosphere and

the troposphere (Solomon et al. 2007; Forster et al. 2010). Stratospheric reduction in the concentrations of ozone, particularly in the Antarctic lower stratosphere as a result of ODS emissions, was discovered in the 1970s/1980s and the Montreal Protocol adopted in 1987 led to the dramatic reduction of ODS emissions (Morgenstern et al. 2008; Forster et al. 2010). Tropospheric effects of the Antarctic ozone hole, however, remained less well investigated until the 2000s, when it became evident that the Antarctic ozone hole affected the circulation and climate in the SH troposphere (Morgenstern et al. 2008; Forster et al. 2010).

Many of the SH climate changes observed over the last century have been attributed to both changes in greenhouse gas forcing and ozone forcing, although the relative importance of these two forcings is still an area of active research, especially for the future climate. It is predicted that future greenhouse gas forcing will continue in the same direction with continuing emissions of greenhouse gases (Solomon et al. 2007), whilst stratospheric ozone forcing trends will reverse due to the implementation of the Montreal Protocol (Morgenstern et al. 2008; Austin et al. 2010; Forster et al. 2010).

2.2 Stratospheric ozone changes

The Montreal Protocol on substances that deplete the ozone layer was adopted in 1987, after recognition that ODSs caused stratospheric ozone depletion, to protect global ozone and thereby to protect life from increased ultraviolet radiation at the earth's surface (Forster et al. 2010). It has successfully controlled anthropogenic emissions of ODSs since its adoption, and the atmospheric concentrations of most major ODSs that were initially controlled by the Protocol are now declining (Forster et al. 2010). However, due to the long atmospheric lifetimes of ODSs, ozone concentrations in the stratosphere are predicted

to remain below 1980 levels for several decades into the 21^{st} century (Forster et al. 2010).

A negative trend in globally averaged TCO was observed from 1980 to the mid-1990s, however recently this trend appears to have plateaued and a reduction in ODS loading appears to have occurred (Solomon et al. 2007). Since changes have been observed (1980), the largest ozone changes have occurred during late winter and spring over Antarctica (Solomon et al. 2007). Ozone depletion occurs most significantly in the Antarctic region because climatologically low temperatures and the presence of polar stratospheric clouds combined with high chlorine and bromine concentrations produced from photochemical breakdown of ODSs leads to the efficient destruction of ozone (Solomon et al. 2007). Ozone depletion in the Arctic region has been less severe than over the Antarctic, as higher temperatures in the lower stratosphere of this region result in fewer polar stratospheric clouds and thus less efficient ozone destruction (Solomon et al. 2007).

The evolution of stratospheric ozone over the next few decades depends on natural and anthropogenic factors (Solomon et al. 2007) with multimodel projections of stratospheric ozone in the 21^{st} century being somewhat varied. As stratospheric ODS loading decreases, the role of these species in ozone evolution becomes less important and other climate change factors become more important. Specifically, expected increases in stratospheric concentration of greenhouse gases (particularly carbon dioxide) will alter the stratosphere (for example, causing cooling and modifying circulation) affecting ozone levels (Forster et al. 2010). Due to intermodel differences in simulated stratospheric inorganic chlorine, there is variation in the predicted timing of recovery of Antarctic column ozone during spring. It is, however, generally accepted that ozone recovery in the future will take a much longer time than ozone depletion in the past. Recovery to 1980 levels is predicted around the

mid-21st century, although it could occur as late as between 2060 and 2070 (Austin et al. 2010).

2.3 Troposheric influence of stratospheric ozone changes

Ozone loss in the Antarctic lower stratosphere is at its highest during October, however there is a one month lag in the radiative temperature effect associated with this depletion, so the largest stratospheric cold anomaly occurs in November (Karpechko et al. 2008).[1] The temperature anomaly in the polar stratosphere results in an increase in the stratospheric westerly polar vortex via the thermal wind relation (Gillett and Thompson 2003), or equivalently a delay in the winter polar vortex breakdown (Perlwitz et al. 2008). These changes in stratospheric winds couple to the troposphere: the precise mechanisms for this coupling are not well understood, however possible explanations may relate to how stratospheric wave drag impacts surface winds and the role of tropospheric eddy horizontal momentum fluxes (McLandress et al. 2011). Although these mechanisms are not well understood, it is known that the coupling occurs during seasons when the stratospheric polar vortex is perturbed by upward dispersing waves from the troposphere, and these conditions occur during late spring/early summer and during autumn (Thompson and Solomon 2002). Thus the maximum stratospheric temperature anomaly coincides with a time when the changes in the stratospheric polar vortex are coupled to the troposphere, invoking a change in the tropospheric SAM. The most pronounced tropospheric trends occur during austral summer (Thompson and Solomon 2002) however observations and reconstructions also find a trend

[1] Significant cooling trends in the stratosphere during the latter part of the 20th century have been attributed to both increasing concentrations of well-mixed greenhouse gases and decreasing concentrations of ozone, with ozone depletion being by far the dominant forcing in the Antarctic lower stratosphere (Son et al. 2010; McLandress et al. 2011).

towards the positive phase of the SAM index in austral autumn (Karpechko et al. 2008; Fogt et al. 2009).

The SAM is the dominant mode of atmospheric variability in the extratropical SH (Thompson and Wallace 2000). The SAM is characterised by a zonally symmetric "annular" structure and describes the balance of mass between the mid- and high latitudes, with pressure fluctuations occurring on daily through to low frequency time scales (Thompson and Wallace 2000; Marshall 2003). There are different measures of the SAM index such as the difference between normalised zonal-mean sea level pressure between 45°S and 60°S, and the first empirical orthogonal function of atmospheric fields including sea level pressure, 500 hPa geopotential height, surface temperature and zonal wind (Thompson and Wallace 2000; Marshall 2003).

Trends in the SAM index have been identified in reanalysis data in many studies, however there are considerable uncertainties in reanalysis data over the Southern Ocean. Marshall (2003) analysed both observations and reanalysis data, defining an observationally based SAM index using the mean sea level pressure from six stations at both 40°S and 65°S. By confirming trends in the SAM index using station-based observations, he was able to remove major uncertainties associated with trends found using reanalysis data. It was concluded, consistent with the findings of studies based on reanalysis data, that there has been an increase in the SAM index (a shift towards its positive phase) from the mid-1960s to the present (Marshall 2003).

This trend implies that the mean surface pressure in high latitudes is decreasing and the mean surface pressure in mid-latitudes is increasing relative to one another, inducing

an intensification and poleward shift in the extratropical eddy-driven westerly jet. This trend is consistent with circulation changes associated with both a decrease in stratospheric ozone and an increase in the concentrations of atmospheric greenhouse gases (Arblaster and Meehl 2006), although the former is important only in late spring and summer whereas the latter occurs year-round (Perlwitz et al. 2008). It has been found that 20^{th} century climate simulations with increasing greenhouse gases reveal trends in the SAM index of the same sign but considerably weaker magnitude than observations, indicating that ozone depletion has had an important influence on the tropospheric SAM trends (Gillett and Thompson 2003). Shindell and Schmidt (2004) and Arblaster and Meehl (2006) further showed that ozone depletion was the dominant contributor to observed changes in the mid-troposhere in summer while both greenhouse gas and stratospheric ozone forcing played a comparable role at the surface (Karpechko et al. 2008). Perlwitz et al. (2008) and Son et al. (2008) note that the scientific consensus finds the Antarctic ozone hole to be the biggest contributor to the observed tropospheric circulation changes during summer, but has a negligible role during other seasons.

2.3.1 Observed SH climate changes

The observed positive trend in the SAM index over the latter part of the 20^{th} century is associated with various regional climate changes. The trend in the SAM has caused cooling over eastern Antarctica and the Antarctic plateau, and an increase in the length of the sea ice season over much of eastern Antarctica and the Ross Sea. It has also been associated with a warming over the Antarctic peninsula and Patagonia, a retreat of ice shelves over the peninsula and a decrease in the sea ice extent in the Bellingshausen Sea (Thompson and Solomon 2002; Shindell and Schmidt 2004; Gillett et al. 2006). An increase in westerly wind speeds over the Southern Ocean has also been observed and attributed to

the increasing SAM index (Shindell and Schmidt 2004).

Temperature changes in other areas associated with the positive phase of the SAM include cooling over much of Australia and warming over Argentina, Tasmania and the south of New Zealand (Gillett et al. 2006). Changes in precipitation include anomalously dry conditions over southern South America, New Zealand and Tasmania and anomalously wet conditions over much of Australia and South Africa. The decreases in precipitation (with the largest responses in Tasmania and southern New Zealand) are centred around 45°S. These decreases are consistent with decreases found in global climate model simulations and are associated with increased geopotential height, subsidence and reduced cloudiness as well as a poleward shift in storm tracks away from this area (Gillett et al. 2006).

Consistent with the findings of Gillett et al. (2006), Hendon et al. (2007) found correlations between the SAM index and daily variations in Australian rainfall and surface temperatures during both austral summer and winter. Variations in the SAM were found to account for approximately 15 % of the weekly rainfall variance in some regions (Hendon et al. 2007). Ummenhoffer et al. (2009) investigated causes of trends in precipitation in New Zealand during the late 20^{th} century and found that a decrease in summer precipitation can be partially explained by the positive phase of the SAM index, with the SAM accounting for up to 80 % and 20–50 % of the overall decline in summer precipitation in the North Island and the western region of the South Island, respectively (Ummenhoffer et al. 2009).

There is also observational evidence that the Hadley cell has widened by about 2–5° latitude since 1979 (Johanson and Fu 2009; Seidel et al. 2008). This change cannot

be explained by natural variability and the observed widening is significantly larger than predicted by global climate model simulations (Johanson and Fu 2009). Such changes are significant because a widening of the Hadley cell implies the poleward movement of large-scale atmospheric circulation systems such as jet streams, storm tracks and changed precipitation patterns (refer to Figure 2.1), which can affect natural ecosystems, agriculture and water resources (Seidel et al. 2008).

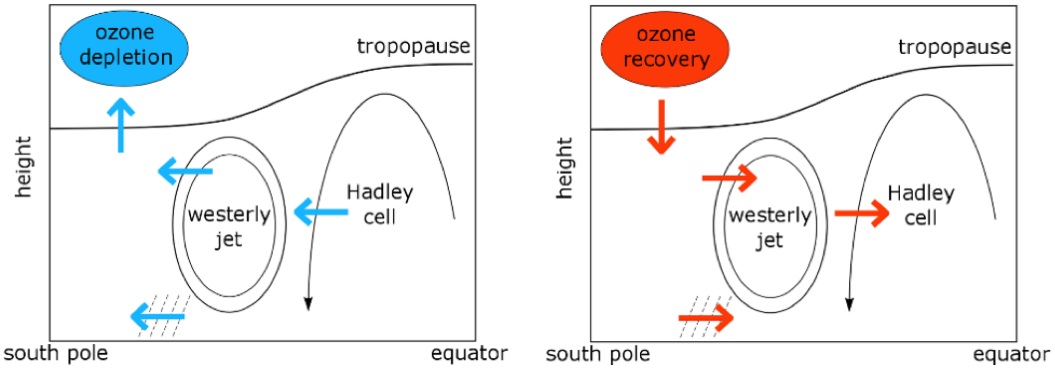

Figure 2.1: Schematic representation of the impact of stratospheric ozone changes on tropospheric circulation in SH summer, from Son et al. (2010). Changes in extratropical tropopause height, location of the westerly jet and storm tracks, and poleward boundary of the Hadley call are shown. The panel on the left shows impacts during ozone depletion and the panel on the right shows impacts during ozone recovery.

2.3.2 Model simulations of SH climate changes

A number of model studies have been undertaken to investigate SAM variability and trends in past and future climates, as well as the relative importance of ozone forcing and greenhouse gas forcing on these changes. Studies discussed here fall into three categories: multimodel studies of CMIP3 model output, multimodel studies of chemistry-climate models participating in the Stratospheric Processes and their Role in Climate /

Chemistry-Climate Model Validation projects (SPARC/CCMVal) and tailored model studies designed specifically for investigating how models respond to the two different forcings.

Cai and Cowan (2007) assessed trends in SH circulation for the second half of the 20^{th} century using 21 CMIP3 models (of which 16 were the same as this study). They found that the modelled trends in austral summer were principally congruent with the modelled trend in the SAM index and that the majority of models produced a statistically significant positive trend in the SAM index over the period of analysis. Separating models into two groups based on ozone forcing (those that prescribed depletion and those that did not) they found that without ozone depletion, the SAM index trend was less than half of that found in corrected reanalysis data, but when ozone depletion was accounted for, the trend was comparable to that of the reanalysis data.

Karpechko et al. (2008) conducted a multimodel study using output from 21 CMIP3 models (of which 17 were the same as in this study) using 20C3m runs and demonstrated that only models that prescribed ozone depletion were able to simulate the observed downward propagation of circulation changes from the stratosphere to the troposphere.

Fogt et al. (2009) examined SAM variability in 17 CMIP3 models (of which 12 were the same as in this study) for the 20C3m and A1B scenario runs and found that the models capture the recent (1957–2005) positive SAM index trends in austral summer. Ozone depletion was attributed as the dominant mechanism driving these trends. Additionally, significant trends in austral autumn were observed: model trends for this season during 1957–2005 were the most different from observations.

Son et al. (2009) also examined model output from 20 CMIP3 models (of which 15 were the same as in this study) for the 20C3m and A1B scenario runs and concluded that stratospheric ozone affects the entire atmospheric circulation in the SH from the polar regions to the subtropics, and from the stratosphere to the surface. Trends attributed at least in part to ozone forcing were detected in stratospheric polar temperature, tropopause heights, jet location, Hadley cell width, SAM index, high latitude precipitation and Antarctic surface temperature (refer to Figure 2.1).

Perlwitz et al. (2008) used a chemistry-climate model to study trends in the SAM index and noted that because the Antarctic ozone hole is expected to recover more slowly than its onset, circulation trends associated with the depletion and recovery phases will occur over different time periods (approximately 30 years and 90 years respectively). They also found that in the 21^{st} century ozone recovery effects dominate trends in the SH tropospheric circulation and oppose the greenhouse gas effects on the SAM index, resulting in an overall decrease in the summer SAM index during this time. However, it was noted that the relative contributions of ozone recovery and greenhouse gas increases on tropospheric circulation were sensitive to the greenhouse gas scenario.

Son et al. (2008) assessed the impact of stratospheric ozone recovery on the SH westerly jet with a set of chemistry-climate models participating in the SPARC/CCMVal-1. As a result of ozone recovery, this study predicted that the tropospheric westerlies in SH summer will be decelerated on the poleward side during the 21^{st} century. In this study it was noted that, although the maximum stratospheric wind anomalies associated with ozone decline occur in November, during the recovery phase they occur during December.

Son et al. (2010) further assessed the impact of stratospheric ozone changes with chemistry-climate models participating in the SPARC/CCMVal-2. They found that stronger ozone depletion in late spring generally leads to greater poleward displacement and intensification of the tropospheric mid-latitude jet and greater expansion of the SH Hadley cell in the summer. However, additional investigation into model bias in the jet location found that the poleward intensification of the westerly jet was generally stronger in models whose climatological jet was biased toward lower latitudes.

In summary, both CMIP3 and chemistry-climate multimodel studies investigating the influence of the Antarctic ozone hole on SH climate have been useful in determining that ozone depletion is required to account for the magnitude of the observed trends in SH circulation during the 20^{th} century. Such studies are also useful as they create averages from different models, which allows common variability to emerge that is unlikely to have arisen from unforced fluctuations, enabling a comparison of the effects of varying ozone forcing to those of increasing greenhouse gases alone.

Other modelling studies, specifically designed to investigate the relative importance of ozone forcing and greenhouse gas forcing, have also been undertaken. For example, Polvani et al. (2011) investigated the relative importance of ozone depletion and greenhouse gas forcing in the second half of the 20^{th} century using an atmospheric general circulation model with prescribed sea surface temperatures and sea ice concentrations, performed with time slice integrations. They found that during SH summer the impacts of ozone depletion on SH circulation were roughly two to three times larger than those of greenhouse gas forcing, in agreement with CMIP3 multimodel-means found in Son et al. (2010).

McLandress et al. (2011) also investigated the relative importance of ozone depletion and greenhouse gas forcing on SH tropospheric climate changes using a version of the Canadian Middle Atmosphere Model, looking at past (1960–1999) and future (2000–2099) climates. They found that the response to ODS occurs primarily in austral summer, and that greenhouse gas forcing produces more seasonally uniform trends with the same sign in the past and future. The response of the two forcings (ozone depletion/recovery and greenhouse gases) was found to be additive, and it was noted that the fact that tropospheric circulation changes were largest in austral summer strongly indicates that stratospheric ozone depletion has played an important role in SH climate change. Increasing high latitude precipitation was found, consistent with the shift in the tropospheric jet which moves storm tracks. Stronger precipitation trends in the past were attributed primarily due to ozone depletion and weaker trends in the future due to increasing greenhouse gases. In general past summer trends were found to be dominated by ODS forcing but future summer trends were influenced by both ODS and greenhouse gas forcings, approximately equally. A comparison to the results of Son et al. (2009) revealed good quantitative agreement of trends in lower stratosphere polar cap temperature, tropopause pressure, jet location, Hadley cell boundary, SAM index and high latitude precipitation.

2.3.3 Biases in model simulations: location of jet

Trends in the SAM explain many changes in SH climate, however as noted by Son et al. (2010), CMIP3 models have some bias in the location of the eddy-driven westerly jet and this leads to a bias in the persistence of the SAM and its trends.

Barnes and Hartmann (2010) investigated the effect of the latitudinal location of the SH eddy-driven westerly jet on the persistence of north/south shifts in the jet using 12

CMIP3 models over four different climate change scenarios. They found that the majority of models placed the mid-latitude jet too close to the equator and that these models had annular modes that were too persistent when compared with observations. Additionally, they found that the equatorward shifted jet was more persistent than the poleward shifted jet and so the persistence of the SAM decreased when the mean jet was located closer to the pole. It was suggested that this occurs because the sphericity of the earth inhibits wave breaking on the poleward flank of the jet and for a poleward displaced jet, this decreases the feedback between eddies and mean-flow and yields a wider, less self-sustaining jet. This implies that models with jets too far equatorward relative to observations over-predict the timescale of the SAM and would exaggerate poleward shifts of jets associated with anthropogenic climate change.

Kidston and Gerber (2010) also investigated the differences in the projected magnitude of jet-shift trend in the SH and found they were well correlated with the biases in the latitude of the jet in 20C3m simulations from 11 CMIP3 models (of which 10 were the same as this study). Like Barnes and Hartmann (2010), Kidston and Gerber (2010) found that an equatorward bias in the position of the jet was associated with both enhanced persistence of the annular mode and an increased poleward shift of the jet. They also found that poleward shifts of the eddy-driven jet stream project onto the positive phase of the SAM index. They described this result physically as the jet stream simply having more room to shift poleward in models that begin with an equatorward bias and so appearing to be more sensitive to external forcing.

2.4 Precipitation and climate change

In the previous sections the possible impact of stratospheric ozone change on tropospheric circulation (eg. on the westerly jet and Hadley cell) and surface climate changes in austral summer (eg. on sea level pressure and surface temperature) were reviewed. This section reviews ozone induced changes in SH hydrology, focussing on seasonal mean and extreme precipitation. Precipitation is one of the most important climate variables and changes in precipitation patterns and variability are likely to have a significant impact on society and ecosystems as well as on global climate by inducing further climate changes.

2.4.1 Observed changes in precipitation

Although trend detection is difficult as precipitation is highly variable spatially and temporally and data are limited in some regions, long term trends in precipitation have been detected over large regions from observations (Solomon et al. 2007). Changes in precipitation in both hemispheres have been observed and an increased variance of precipitation is found in observations across the globe (Dore 2005). Consistent with warming and the associated increase in atmospheric water vapour, heavy precipitation events have become more frequent over most land areas (Solomon et al. 2007; Min et al. 2011). For many regions, an increase in mean precipitation is disproportionately reflected in increased heavy precipitation, and for some regions where the mean decreases, heavy precipitation has still increased (Dore 2005).

Changed precipitation patterns over the ocean can alter the density of surface water, affecting deep water formation and global ocean circulation and thus having important consequences to global climates. Changes in the net freshwater flux (P–E) over the oceans is suggested by observed freshening of mid- and high latitude waters and increased salinity

of low latitude waters in the SH (Solomon et al. 2007). As well as these observed surface changes, Antarctic intermediate water and sub-Antarctic mode water have become fresher, cooler and deeper, consistent with an increased freshwater flux in the source regions of such waters (Dore 2005).

2.4.2 Global climate models and precipitation

Simulations of the 21^{st} century climate suggest that mean precipitation will increase in the tropics and extratropics, and decrease in the subtropics. That is, wet areas will get wetter and dry areas will get drier (Dore 2005). Precipitation extremes, however, are expected to increase almost across the globe (O'Gorman and Schneider 2009).

It is important to understand how well global climate models reproduce precipitation patterns and trends before conclusions from simulations are drawn. Dai (2006) described the precipitation characteristics of 18 coupled climate models (of which 16 were the same as used in this study) from 20C3m simulations based on monthly and three-hourly mean data. Most models reproduced the observed patterns of precipitation amount and interannual variability, and the percentage contribution and frequency for moderate precipitation (10–20 mm day^{-1}) reasonably. However, models underestimated the contribution and frequency for heavy precipitation (>20 mm day^{-1}) and overestimate them for light precipitation (<10 mm day^{-1}). From this, it is evident that the current generation of climate models require improvements in precipitation simulations. However taking note of typical shortcomings of climate models, precipitation data from global climate models can still be useful if general changes and trends are considered, whilst keeping limitations of precipitation predictions in mind. It should also be noted that significant uncertainties also exist in merged precipitation data, such as CPC Merged Analysis of Precipitation (CMAP)

and Global Precipitation Climatology Project Version-2 (GPCP v2) data sets, due to wind induced under-catch by rain gauges and uncertainties in satellite observations (Dai 2006). Model precipitation is found to be closer to GPCP v2 than CMAP in mid- and high latitudes (Dai 2006).

Changes in the synoptic environment south of 40°S have been observed over recent decades, with a notable poleward shift in baroclinicity (Fyfe 2003). South of 60°S a modest increase in the number of cyclones has been observed, however between 40–60°S the number of cyclones has dramatically decreased (Fyfe 2003). Lambert and Fyfe (2006) examined the changes in total number of cyclone events, and number of intense events, for 15 CMIP3 models (of which 13 were the same as this study) and found that models robustly simulate a reduction in total events and an increase in intense events with a warming climate.

Held and Soden (2006) analysed model output from CMIP3 models and found an enhancement in the P–E pattern and its temporal variance. They found that the poleward movement of storm tracks displaced the poleward boundary of the dry subtropical zones with P–E < 0 farther poleward. They also noted discrepancies in predictions over the Southern Ocean, where a reduction in evaporation occurred and the increase in poleward moisture flux was underestimated. Bengtsson and Hodges (2006) found that in the SH a clear poleward shift of $\sim 5^\circ$ in storm tracks was predicted in all seasons, however the statistical distribution of storm intensities was virtually preserved in the 21^{st} century for the A1B scenario. The greatest reduction in the number of storms occurred around 40°S during austral winter, and the greatest reduction in storm activity occurred around 50°S in austral summer, with a corresponding increase in storm activity around 60°S. During summer a general weakening of storm intensities was found, whereas in winter an increase

in intensities was found.

Sun et al. (2007) used daily data from 17 CMIP3 models (of which 15 were the same as used in this study) for the B1, A1B and A2 scenarios during the 21^{st} century to investigate changes in precipitation characteristics. They found that all models consistently show a shift toward more intense and extreme precipitation for the globe as a whole and over various regions. This increase in extreme precipitation was expected, as tropospheric warming associated with increased greenhouse gases leads to an exponential increase in the water-holding capacity of the atmosphere of $\sim$7 % K^{-1} (based on the Clausius-Clapeyron relation). This implies, based on little changes in relative humidity, an exponential increase in atmospheric moisture content. However, the overall intensity of the global hydrological cycle is controlled by the surface energy balance. Due to energy limitations, extreme precipitation cannot increase unchecked with the increasing atmospheric moisture content. Thus, if extreme precipitation is increasing, there must be a decrease in the frequency or intensity of light or moderate precipitation events to balance the energy budget.

To further investigate the predicted changes in precipitation in the 21^{st} century, Sun et al. (2007) classified daily precipitation into commonly used categories (very light 0.1–1 mm day^{-1}, light 1–10 mm day^{-1}, moderate 10–20 mm day^{-1}, heavy 20–50 mm day^{-1}, and very heavy >50 mm day^{-1}) and investigate changes in the frequency and intensity of these categories. They found that models overestimate the frequency of precipitation for less than $\sim$20 mm day^{-1} and underestimate it for more than $\sim$20 mm day^{-1}: precipitation occurs too frequently at reduced intensity in climate models. The changes in total and light (1–10 mm day^{-1}) precipitation frequency were found to be very similar, because light precipitation makes up a significant component of total precipitation in climate models (more

than 40 %, which is too high a proportion compared to observations). Large increases in precipitation frequency were observed in the high latitudes, however the frequency of very light precipitation (0.1–1 mm day^{-1}) decreased around 65°S.

Sun et al. (2007) also looked at changes in surface latent heat fluxes and found that in the 21st century models predict it will increase in most part of the globe, however in areas of the Southern Ocean and southern Africa, this was not found to be the case.

2.4.3 Precipitation extremes

Increases in extreme precipitation events have already been observed (Min et al. 2011) and are predicted for the future (Emori and Brown 2005; Kharin et al. 2007; O'Gorman and Schneider 2009). As mentioned above, future increases in extreme precipitation events are also accompanied by a reduction in the probability of wet days, implying more likely floods and droughts in the future (Kharin et al. 2007).

Emori and Brown (2005) investigated the changes in mean and extreme precipitation in a warming climate separating dynamic effects (due to changes in atmospheric motion) and thermodynamic effects (due to changes in atmospheric water content). They used four CMIP3 models (also used in this study) and two additional time slice climate change experiments by atmosphere-only models. They found that models consistently showed an increase in mean precipitation over the tropics and mid- to high latitudes and decreases over some subtropical regions, with thermodynamic changes accounting for the changes in the mid- to high latitudes. These findings were consistent with other studies. They also found that changes in extremes were similar to changes in the mean, but there are some areas where extremes increase more than the mean. As with mean precipitation,

thermodynamic effects were found to dominate changes in extreme precipitation. In the extratropics, dynamic effects were found not to be important in terms of changes in extreme precipitation.

O'Gorman and Schneider (2009) also investigated changes in extreme precipitation using output from 11 CMIP3 models (of which 10 were the same as this study) from the 20C3m and A1B scenario runs. Comparing the 99.9^{th} percentile of daily precipitation within grid boxes, they found that in the extratropics precipitation extremes consistently increased more slowly than atmospheric water content. Factors affecting changes in extremes were separated into changes in the moist adiabatic lapse rate, changes in upward velocity, and changes in temperature when the precipitation extreme occurred. The fact that, as the climate warmed, the observed increase in precipitation extremes was smaller than the increase in water vapour content was viewed as a consequence of static stability changing more slowly with temperature than the saturation specific humidity. To test this theory, a scaling to describe changes in precipitation was developed to describe the intensity of precipitation extremes at a given latitude:

$$P_e \sim -\left\{ \omega_e \left. \frac{dq_s}{dp} \right|_{\theta^*, T_e} \right\} \tag{2.1}$$

where P_e is the high percentile of precipitation, ω_e is the corresponding upward vertical velocity, $\{.\}$ is a mass-weighted integral over the troposphere, and the moist-adiabatic derivative of saturation specific humidity ($\frac{dq_s}{dp}$) is evaluated at the conditional mean temperature T_e when extreme precipitation occurs. This scaling captured all the behaviour of precipitation extremes at all latitudes in the multimodel mean. The scaling was simplified by omitting ω_e from the equation to give a purely thermodynamic scaling which was found to give good agreement in the extratropics. This indicated, consistent with the findings of

Emori and Brown (2005), that in the extratropics, thermodynamic effects control changes in precipitation extremes. The agreement with theory and consistency amongst climate models in the extratropics increased confidence in the robustness of results.

2.4.4 Hydrological influences of stratospheric ozone changes

Previous studies, as described above, focus mainly on hydrological climate changes associated with anthropogenic warming. To date, no quantitative investigation with multimodel data sets has been conducted, although ozone-induced hydrological changes have been proposed in several studies (Son et al. 2009; McLandress et al. 2011; Polvani et al. 2011). Thus, this study aims to bridge the existing gap in understanding the effects of anthropogenic climate change on the hydrological cycle, by quantitatively investigating ozone-induced impacts on precipitation and evaporation.

Chapter 3
Methodology

To achieve the objectives of this project and investigate the influence of ozone-induced climate change on SH hydrology, two data sources are utilised in analysis: observations and model output.

3.1 Observations

Observation data sets for precipitation and evaporation from 1979–2008 are used to calculate 20^{th} century climatologies. Observation seasonal climatologies are then compared to model climatologies. Detailed trend analysis is not possible with the merged observational data sets used because of uncertainties in observations and merging algorithms, but time series of zonally averaged precipitation and evaporation are compared to TCO trends to make a qualitative comparison.

3.1.1 Total column ozone

The National Institute of Water and Atmospheric Research Version-2 assimilated TCO data (Bodeker et al. 2005) is used to determine trends in stratospheric ozone concentration from 1979–2008. This data set combines satellite-based ozone measurements from four total ozone mapping spectrometer instruments, three different retrievals from the global ozone monitoring experiment and data from four solar backscatter ultra violet instruments. Comparison with the ground-based Dobson spectrophotometer network shows its reliability.

Trends in ozone are determined by plotting a time series of the area-weighted TCO averaged over 60–90°S for October (when ozone decline is most pronounced). This time series is then compared to the time series constructed for precipitation and evaporation observations.

3.1.2 Precipitation

The GPCP v2 monthly precipitation analysis data set (Adler et al. 2003) is used as the precipitation reference climatology. This is a global data set of surface precipitation at 2.5° latitude by 2.5° longitude resolution, available from January 1979 to the present. It is a merged analysis incorporating precipitation estimates from surface rain gauge observations, low-orbit satellite microwave data and geosynchronous-orbit satellite infrared data.

Seasonal climatology maps using data from 1979–1999 inclusive are constructed for comparison with the model climatology maps. Seasons are defined as summer (December, January and February, hereinafter referred to as DJF), autumn (March, April and May, hereinafter referred to as MAM), winter (June, July and August, hereinafter after referred to as JJA) and spring (September, October and November, hereinafter after referred to as SON).

3.1.3 Evaporation

The Objectively Analyzed Air-Sea Heat Fluxes (OAFlux) Version-3 global ocean evaporation data set (Yu et al. 2008) is used as the reference evaporation climatology. This is a global data set of ocean evaporation at 1° latitude by 1° longitude resolution available from 1958–2008. It is a merged data set constructed from an optimal blending of satellite

retrievals and three atmospheric reanalyses.

This data set is treated in the same way as the GPCP v2 precipitation data set. Seasonal climatology maps using data from 1979–1999 inclusive are constructed for comparison with the model climatology maps. Seasonal zonal-mean time series are also constructed for 1979–2008 (consistent with the analysis period of precipitation data), and averaged over the same latitudinal extents.

3.2 CMIP3 data

Model output from the CMIP3 multimodel database is analysed for trends in precipitation, evaporation and other fields of interest in the 20^{th} and 21^{st} centuries. A total of 19 models are used in this study: the models employ different dynamical equations, physical parametrisations of the atmosphere and ocean, sea ice dynamics and leads, coupling adjustments, and land and surface components. The salient details of the atmospheric component of each model used in this study are shown in Table 3.1. The reader is referred to Randall et al. (2007) for further information on individual models. All models prescribed stratospheric ozone with a seasonal cycle. Additionally, some models prescribed the ozone concentration decline in the latter part of the 20^{th} century and recovery in the 21^{st} century. Of the 19 models used, roughly half (10 models) incorporated ozone depletion and ozone recovery, whilst the other half (nine models) simply prescribed climatological ozone fields. Although there were more models archived in CMIP3, several CMIP3 models are excluded in this study. These models are listed in Table 3.2 and the reasons for their exclusion are briefly outlined there.

The actual ozone fields used by the different models were not archived, and the ozone depletion and recovery characteristics varied amongst the 10 models which included it, thus a detailed intermodel comparison of how ozone forcing affects precipitation and evaporation using CMIP3 models is not possible. Therefore, as with previous studies, the models used in this study are grouped into four categories that broadly describes the ozone fields employed. This classification is based on previous work (Cai and Cowan 2007; Karpechko et al. 2008; Fogt et al. 2009; Son et al. 2009), which assessed trends in stratospheric polar temperatures to determine whether ozone concentrations declined in the 20^{th} century (strong cooling trend) or not (almost no trend) and recovered in the 21^{st} century (strong warming trend) or not (almost no trend). In this study all models with ozone depletion in the 20^{th} century also incorporated ozone recovery in the 21^{st} century and hereinafter are collectively referred to as models with "varying ozone forcing". Likewise models without ozone depletion in the 20^{th} century also lacked ozone recovery in the 21^{st} century and hereinafter are collectively referred to as models with "fixed ozone forcing". Data for the 20^{th} century are obtained from the 20^{th} century experiment (20C3m) and for the 21^{st} century from the special report on emissions scenarios A1B experiment (A1B).

In all analysis, data are grouped by season: DJF, MAM, JJA and SON. Ensemble averages of trends and climatologies are created for each model. Seasonal trends and climatologies are linearly interpolated to a standard grid of 2° latitude by 2° longitude, consistent with previous multimodel comparisons by Son et al. (2009). Each model is weighted equally and multimodel averages are created for each model group. Hatching is used on trend maps to denote where the multimodel mean trend is greater than or equal to one standard deviation of the trends of different models within that group.

Table 3.1: Description of CMIP3 models used in this study. Details of each model are described in Randall et al. (2007), except CSIRO-Mk3.5 described in Gordon et al. (2010) and INGV-SXG described in Scoccimarro et al. (2007). Horizontal resolution is approximate for spectral models, where "T" refers to triangular truncation.

Model	Group	Country	Atmospheric Resolution			Varying Ozone
			Horizontal (lat. × lon.)	Vertical Levels	Top (hPa)	
CCSM3.0	NCAR	USA	T85 (1.4° × 1.4°)	26	2.2	Yes
CSIRO-Mk3.0	CSIRO	Australia	T63 (1.9° × 1.9°)	18	4.5	Yes
CSIRO-Mk3.5d	CSIRO	Australia	T63 (1.9° × 1.9°)	18	4.5	Yes
ECHAM5/MPI-OM	MPI	Germany	T63 (1.9° × 1.9°)	31	10	Yes
GFDL-CM2.0	NOAA	USA	2.0° × 2.5°	24	3	Yes
GFDL-CM2.1	NOAA	USA	2.0° × 2.5°	24	3	Yes
INGV-SXG	INGV	Italy	T106 (1.1° × 1.1°)	19	10	Yes
MIROC3.2(hires)	CCSR	Japan	T106 (1.1° × 1.1°)	56	40 km	Yes
MIROC3.2(medres)	CCSR	Japan	T42 (2.8° × 2.8°)	20	30 km	Yes
PCM1.1	NCAR	USA	T42 (2.8° × 2.8°)	26	2.2	Yes
BCCR-BCM2.0	BCCR	Norway	T63 (1.9° × 1.9°)	16	25	No
CGCM3.1(T47)	CCCma	Canada	T47 (2.8° × 2.8°)	31	1	No
CGCM3.1(T63)	CCCma	Canada	T63 (1.9° × 1.9°)	31	1	No
CNRM-CM3	CNRM	France	T63 (1.9° × 1.9°)	45	0.05	No*
ECHO-G	MIUB	Germany/Korea	T30 (3.9° x 3.9°)	19	10	No
GISS-AOM	NASA	USA	3.0° × 4.0°	12	10	No
INM-CM3.0	INM	Russia	4.0° × 5.0°	21	10	No
IPSL-CM4	IPSL	France	2.5° × 3.7°	19	4	No
MRI-CGCM2.3.2	MRI	Japan	T42 (2.8° × 2.8°)	30	0.4	No

* Model documentation claims inclusion of ozone chemistry, however analysis of Antarctic polar-cap temperature by Son et al. (2008) found no ozone impact in either 20C3m or A1B simulations

Modelling group acronyms are:
NCAR - National Center for Atmospheric Research
CSIRO - Commonwealth Scientific and Industrial Research Organisation Atmospheric Research
MPI - Max Planck Institute for Meteorology
NOAA - National Oceanic and Atmospheric Administration / Geophysical Fluid Dynamics Laboratory
INGV - Istituto Nazionale di Geofisica e Vulcanologia
CCSR - Center for Climate System Research
BCCR - Bjerknes Centre for Climate Research
CCCMA - Canadian Centre for Climate Modelling and Analysis
CNRM - Centre National de Recherches Météorologiques / Météo-France
MIUB - Meteorological Institute of Bonn and Korea Meteorological Administration
NASA - National Aeronautics and Space Administration / Goddard Institute for Space Studies
INM - Institute for Numerical Mathematics
IPSL - Institut Pierre Simon Laplace
MRI - Meteorological Research Institute

Table 3.2: CMIP3 models excluded in this study.

Model	Group	Country	Comments
BCC-CM1	BCC	China	No precipitation or surface latent heat flux data available
FGOALS1.0g	IAP	China	Monthly precipitation data for 20^{th} century in the high latitude region found to be unreasonably higher than observations and all other models
GISS-EH	NASA	USA	Daily precipitation data not available for 21^{st} century
GISS-ER	NASA	USA	Daily precipitation data for 20^{th} century between 1971–1999 found to be erroneous: data is approximately seven times greater than all other models
UKMO-HadCM3	UKMO	UK	Daily precipitation data not available for 20^{th} and 21^{st} centuries
UKMO-HadGEM1	UKMO	UK	Daily precipitation data not available for 20^{th} and 21^{st} centuries

Modelling group acronyms are:
BCC - Bejing Climate Center
IAP - Institute of Atmospheric Physics
UKMO - UK Met Office / Hadley Centre for Climate Prediction and Research

3.3 Model analysis: monthly-mean data

Monthly precipitation (P) and surface latent heat flux data are directly obtained from the CMIP3 archive. Surface latent heat flux is then converted to evaporation (E) using a simple formula presented in Equation 3.1. All analyses are conducted across the SH as the ozone-induced climate change in the northern hemisphere are negligible (Son et al. 2009). The seasonal mean trends for each model group are determined using least squares: in the 20^{th} century over the period 1960–1999 and in the 21^{st} century over the period 2000–2079. Note that for the 20^{th} century, climatologies are calculated for the period 1979–1999 to be consistent with the observational climatologies. Here, 40-year and 80-year periods are chosen to capture changes in stratospheric ozone and surface hydrology, whilst being as long as possible to improve statistics. The longer analysis period in the 21^{st} century is chosen as ozone recovery is expected to occur over a longer period than ozone depletion (eg. Austin et al. 2010).

3.3.1 Precipitation (P)

For monthly-mean precipitation analysis, data from 19 models are analysed with the number of runs per model ranging from one to five, as outlined in Table 3.3. To ensure consistency between monthly and daily data analyses, only the ensemble members with both monthly and daily data available are used. Since less data from the daily data set are typically available and/or suitable for analysis, several ensemble members with only monthly-mean data are excluded from monthly analysis.

Table 3.3: Ensemble members of 20C3m and A1B simulations used in the analyses of precipitation (precip.), evaporation (evap.) and 925 hPa zonal wind (u-wind). Ensemble members used for P–E analysis are the same as for evaporation.

Model	**Number of Ensemble Members Analysed**					
	20C3m precip.	**A1B precip.**	**20C3m evap.**	**A1B evap.**	**20C3m u-wind**	**A1B u-wind**
CCSM3.0	4	5*	4	5	4	5
CSIRO-Mk3.0	3	1*	3	1	2	1
CSIRO-Mk3.5d	3	1*	3	1	3	1
ECHAM5/MPI-OM	2	2*	2	2	2	2
GFDL-CM2.0	1	1*	1	1	1	1
GFDL-CM2.1	1	1*	0	0	1	1
INGV-SXG	1	1*	1	1	1	1
MIROC3.2(hires)	1	1*	1	1	1	1
MIROC3.2(medres)	2	3*	1	3	2	3
PCM1.1	3	1*	3	1	3	1
BCCR-BCM2.0	1	1	1	1	1	1
CGCM3.1(T47)	5	3*	3	3	5	3
CGCM3.1(T63)	1	1*	1	1	1	1
CNRM-CM3	1	1	1	1	1	1
ECHO-G	3	3*	3	3	3^x	3^x
GISS-AOM	1	1*	1	1	1	1
INM-CM3.0	1	1*	1	1	1	1
IPSL-CM4	2^+	1	2	1	2	1
MRI-CGCM2.3.2	5	5*	5	4	5	5

* Indicates A1B data sets begin at 2001 (rather than 2000)

+ Indicates one run of this ensemble starts at 1961 (rather than 1960)

x Indicates surface zonal wind data is used (pressure-level data is not available)

3.3.2 Evaporation (E)

Surface latent heat flux is converted to evaporation and analysed in the same way as precipitation data. With no latent heat flux data from GFDL-CM2.1 (refer to Table 3.3), only 18 models are analysed for evaporation (nine models in each ozone forcing group).

Conversion from latent heat flux to evaporation is carried out by assuming:

1. Constant density of surface seawater = 1026 kg m^{-3}; and
2. Constant sea surface temperature (SST) = 15°C.

The first assumption is taken to be reasonable as the change in surface seawater density with latitude is small, ranging from 1022–1027 kg m^{-3} (Brandon 2010). To assess the second assumption the OAFlux evaporation data, which incorporates climatological SSTs, is converted to latent heat flux by using NOAA Extended Reconstructed SST V3b data. A constant SST is then used to re-convert latent heat flux back to evaporation, giving a "modified" observation set. This modified evaporation data is compared to the original OAFlux evaporation data to find the importance of spatial and time varying SSTs. The difference between the two data sets is found to be negligible. Thus the second assumption is considered reasonable.

Based on the above assumptions, surface latent heat flux is converted to evaporation (first in m s^{-1} and from that to mm day^{-1}) as described in Yu et al. (2008):

$$E = \frac{Q_{LH}}{\rho_w L_e} \tag{3.1}$$

where Q_{LH} is the latent heat flux (W m^{-2}), ρ_w is the density of sea water (kg m^{-3}), and L_e is the latent heat of vaporisation (J kg^{-1}) that can be expressed as:

$$L_e = (2.501 - 0.00237 \times SST) \times 10^6 \tag{3.2}$$

3.3.3 Precipitation minus evaporation (P–E)

To analyse P–E, evaporation (E) of a given model realisation is subtracted from the corresponding precipitation (P) of the same realisation. Thus the models and realisations used in P–E analysis are the same as those used in evaporation analysis (Table 3.3) with nine models in both ozone forcing groups. P–E is then treated as an independent variable and analysed in the same manner as precipitation and evaporation are.

3.4 Model analysis: daily-mean data

To further investigate the effects of ozone-induced climate change on hydrology, the frequency and intensity of precipitation are examined using daily-mean data.

3.4.1 Decadal-difference precipitation

Unfortunately daily-mean data from the A1B experiment is not available continuously from 2000–2079, making trend detection methods used for the monthly-mean data analysis impossible with daily data. Thus a new approach is introduced for daily precipitation analyses: a decadal-difference method. The climatology of three individual decades is determined and the differences between them are analysed. Based on daily precipitation data availability for the 20C3m runs (typically 1961–1999) and for the A1B runs (typically 2046–2065 and 2081–2100), the three decadal periods are chosen as follows:

1. 01/01/1961 to 31/12/1970;
2. 01/01/1990 to 31/12/1999; and

3. 01/01/2056 to 31/12/2065.

Climatology of each decadal period is first computed. Then the difference between the second decade mean (1990–1999) and the first decade mean (1961–1970) is calculated to determine the change the 20^{th} century, reflecting the impact of ozone depletion. The difference between the third decade mean (2056–2065) and the second decade mean (1990–1999) is also calculated to determine the change in the 21^{st} century, in association with ozone recovery. As shown in Chapter 4, although the decadal-difference method is quantitatively different from long-term trend, they are qualitatively similar to each other, allowing conclusions drawn from monthly-mean data analysis to be applied to the daily-mean data analysis.

3.4.2 Precipitation intervals

To gain more insight into the decadal-differences in mean precipitation, frequency and total accumulation of precipitation for different intensity regimes are also investigated. Precipitation intervals are defined as 0.1–1 mm day^{-1} (very light precipitation), 1–10 mm day^{-1} (light precipitation) and >10 mm day^{-1} (moderate to heavy precipitation) as in Sun et al. (2007).

3.4.3 Extreme precipitation

To examine the effect of ozone forcing on extreme precipitation, five extreme precipitation indices are analysed from the Expert Team on Climate Change Detection and Indices (ETCCDI) core climate change indices (Peterson et al. 2001; ETCCDI 2009):

1. SDII: simple precipitation index or daily-mean precipitation intensity, defined as the sum of precipitation on all wet days divided by the number of wet days (where a wet day is defined as a day receiving ≥1 mm of rain-equivalent precipitation);

2. R95pTOT: the sum of rainfall on days exceeding the 95^{th} percentile threshold value, as determined for the base period of 1961–1990;
3. R99pTOT: the sum of rainfall on days exceeding the 99^{th} percentile threshold value, as determined for the base period of 1961–1990;
4. Rx1day: seasonal maximum one-day precipitation; and
5. Rx5day: seasonal maximum five-day consecutive precipitation.

These extreme precipitation indices are standard and have been used in many studies (eg. Meehl et al. (2005) used SDII; Pal and Al-Tabbaa (2009) used R95pTOT, R99pTOT, Rx1day and Rx5day; Bartholy and Pongrácz (2010) used SDII, R95pOT, Rx1day and Rx5day; Mailhot et al. (2010) used Rx1day and Rx5day; and Min et al. (2011) used Rx1day and Rx5day).

3.5 Statistical analysis

Multimodel trends determined above are plotted on polar stereographic maps from 30°S to the pole and trends between model groups are compared visually (refer to Chapter 4). Whilst this is a useful comparison, it is also inherently subjective. It is desirable to be able to compare multimodel trends between the two groups of models (models with varying ozone and models with fixed ozone) statistically, to determine if the trends are significantly different between the two groups. To do this, trends are separately averaged over the mid-latitudes and high latitudes, as these regions showed fairly homogeneous trends in space. Area averages are calculated with respect to the jet location as outlined in Section 3.5.1 and significance tests are described in Section 3.5.2.

3.5.1 Location of jet

Previous studies have shown that the mean precipitation trend for DJF in the 20^{th} century has a dipole pattern with an increasing trend in precipitation from latitudes of approximately 50–55°S all the way to the Antarctic continent (70–80°S), and a decreasing trend in precipitation between latitudes of approximately 35–40°S to 50°S. Both increasing and deceasing trends are homogeneous in the zonal direction although the magnitude of the trends vary slightly.

Rather than specifying absolute latitude limits to calculate the area-mean trends, model-dependent relative limits are considered in this study. As changes in precipitation and evaporation are presumed to be a result of the poleward shift in storm tracks, and as these storm tracks are inherently linked to the location of the extratropical eddy-driven westerly jet, the high and mid-latitude bands can be defined by using the location of the westerly jet within individual models. This approach takes into account the bias in jet location that many models have: studies discussed in Section 2.3.3 have shown that CMIP3 models have a large variation in both the location and intensity of the jet (Son et al. 2010; Barnes and Hartmann 2010; Kidston and Gerber 2010). This bias in jet location and intensity with reference to the National Centers For Environmental Prediction (NCEP)-NCAR reanalysis and the European Centre for Medium-Range Weather Forecasts ERA-40 reanalysis jets is briefly discussed in Section 4.1.3.

The location of the jet is identified by using the 925 hPa zonal-mean zonal wind. Zonal wind data used in this calculation is chosen to be as consistent as possible with precipitation and evaporation data, although exceptions are noted in Table 3.3. Of particular note, pressure-level zonal wind is not available for MIUB ECHO-G, so surface zonal wind is used

to determine the location of the jet in this model. Jet location is simply determined as the location of the maximum zonal-mean zonal wind at 925 hPa[1] for both the 20^{th} and 21^{st} centuries. The average of these two centuries is then taken as the jet location for statistical calculations.

Once the location of the jet is determined in all models, the zonal-mean precipitation climatology and precipitation trends are plotted versus absolute latitude and versus latitude relative to the jet. It can be seen that when plotted relative to the jet, the peaks in precipitation climatology and precipitation trends for different models align more consistently. Based on this result, area-weighted regional-mean values in high latitude and mid-latitude regions are calculated over 4–34°S of the jet and over 10–0°N of the jet, respectively.

3.5.2 Statistical tests

Two statistical tests are used to compare the average values between the groups of models with varying ozone forcing versus with fixed ozone forcing: a Student t-test and a Monte Carlo based approach. For both tests, significant differences between the two groups of models being compared are tested at the 95 %, 99 % and 99.9 % confidence levels. Trends in the high latitude region are treated separately from trends in the mid-latitude region.

[1] Most studies define the location of the jet based on the maximum 850 hPa zonal wind (eg. Son et al. 2010), however 925 hPa zonal wind is used here, to minimise the differences between surface zonal wind used for MIUB ECHO-G.

More specifically, a two-sample t-test is used in this study. It tests the null hypothesis that data in the two groups being compared are independent random samples from normal distributions with equal means and equal but unknown variances, against the alternative that the means are not equal. Both right- and left-tail tests are used to indicate which group of models has the higher mean.

Due to concerns of the applicability of the t-test to small sample sizes (groups of 10 models and nine models) a Monte Carlo approach is also used. From the 19 models used in this study, one group of 10 models and one group of nine models are selected at random, regardless of ozone forcing. The difference between the two means of the randomly selected groups is calculated. This process is repeated 10,000 times to get a distribution of the difference between the means of two randomly selected groups of models. The actual difference between the mean of the varying ozone group and the fixed ozone group is calculated and compared to the distribution of random mean differences: if the actual difference lies in either tail region of the random difference, it is unlikely that the difference occurrs just by chance, indicating statistical significance.

The results of these two significance tests are very similar. In most cases significance is found at the same level. Only in a few cases the significance found with a t-test is a level lower than the significance found with the Monte Carlo test (eg. if the Monte Carlo approach found significance at the 99.9 % level, the t-test found significance at the 99 % level). However, statistical significance of the minimum level tested (95 % level), when found, is always found with both tests.

Chapter 4
Results and discussion

The analysis results are presented and discussed below. First, a climatology assessment is presented, evaluating the ability of each model to simulate precipitation, evaporation and the mid-latitude eddy-driven westerly jet. Next, trends in observations are briefly discussed and compared to trends in models. Following this, multimodel trends are presented and discussed. Finally a discussion of the statistical tests is made. In presenting results, many maps are shown. Although analysis is conducted over the entire extent of the SH, the maps included here only show areas from 30°S to the pole, as no coherent trends are found in the tropics and focusing on the extratropics allows the regions of interest to be seen more clearly. Many figures showing zonal averages are also presented. Such figures include data from individual models and multimodel averages (shown in bold). The purpose of these figures is not to focus on the behaviour of individual models, but rather to focus on each model group as a whole, and to see the spread amongst models in each group. As such, individual models are not specifically identified, but rather colour coded based on their grouping. In this way the reader is encouraged to compare the differences between model groups rather than individual models.

4.1 Climatological assessment

In climatology comparison figures (Figure 4.1 and Figure 4.3), climatology maps are shown with top panels for SH summer (DJF) and bottom panels for SH winter (JJA). Observations are shown on the left, models with ozone depletion in the 20^{th} century in

the centre and models without ozone depletion in the 20^{th} century on the right. These figures show how accurately the multimodel averages simulate the geographic distribution of seasonal-mean precipitation and evaporation. The seasonal cycle of individual models is also compared to that of the observations in Figure 4.2 and Figure 4.4.

4.1.1 Precipitation

Figure 4.1 shows that the major features of the observed precipitation are reasonably well captured by the multimodel averages of both groups of models. When quantitatively compared to the GPCP v2 data, in DJF subtropical regions of high precipitation such as Uruguay and northern Argentina, the western subtropical South Atlantic Ocean and the central subtropical South Pacific Ocean show a smaller amount of precipitation in both groups of models. In JJA the models again underestimate the precipitation over the subtropical western South Atlantic Ocean compared to observations, but overestimate the precipitation over the subtropical South Pacific Ocean. Both groups of models also slightly overestimate ocean precipitation in the extratropical Indian Ocean.

The top panel of Figure 4.2 shows that in high latitudes the models reproduce a reasonable seasonal cycle in zonal-mean precipitation. Except for March, the multimodel averages of both groups of models are similar to the GPCP v2 precipitation. In March the GPCP v2 precipitation is greater than both multimodel averages but is still within the model spread. Although both multimodel averages approximate the GPCP v2 precipitation well, there is a smaller spread in the models with ozone depletion than in the models without ozone depletion. The bottom panel of Figure 4.2 shows that in mid-latitudes the models have more difficulty reproducing the seasonal cycle. As in high latitudes, both multimodel averages are similar and there is a larger spread in the models without ozone depletion. However

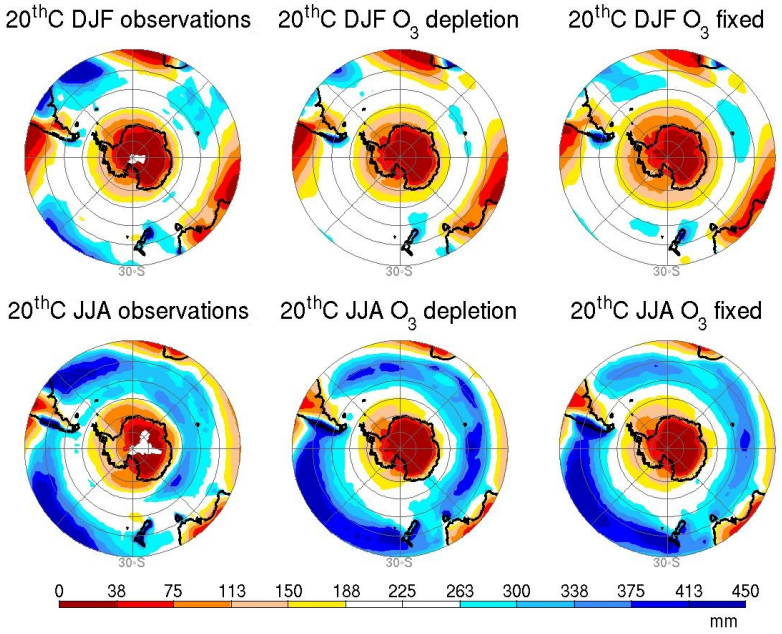

Figure 4.1: Precipitation climatology for 1979–1999. Panels on the left show GPCP v2 observations, in the centre show CMIP3 models with ozone depletion and on the right show CMIP3 models without ozone depletion.

both groups of models have a seasonal variation that is larger than that of the observations. Summer and early autumn precipitation is underestimated by the models and in February observations lie outside the multimodel spread. In winter and early spring, precipitation is overestimated by the models but observations lie within the multimodel spread in this case.

Based on the above assessment it can be concluded that although there are limitations in the individual models' abilities to reproduce the observed precipitation pattern and its seasonality, the multimodel average is able to produce a reasonable precipitation pattern and seasonal cycle especially in high latitudes in both seasons.

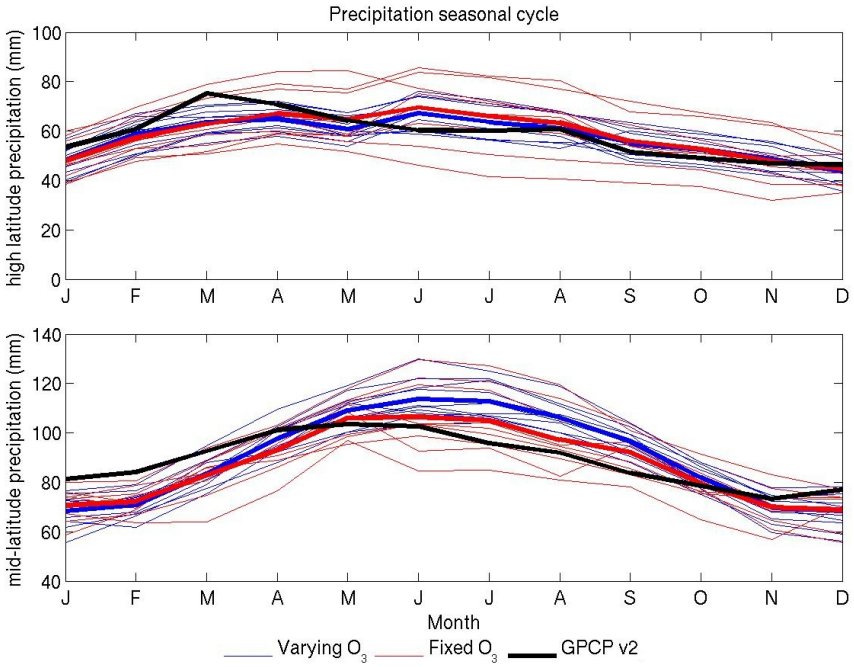

Figure 4.2: Seasonal cycle of zonal-mean precipitation, averaged over 1979–1999, for individual models, multimodel averages and GPCP observations. The top panel shows the seasonal cycle averaged over high latitudes (4–34°S of the jet) and the bottom panel shows the seasonal cycle averaged over mid-latitudes (10–0°N of the jet). Models with varying ozone forcing are shown in blue and models with fixed ozone forcing are shown in red. The multimodel averages of the respective groups are shown in bold. Observations are shown in bold black. This colour convention is used consistently in following figures.

4.1.2 Evaporation

Figure 4.3 shows that the multimodel averages capture the spatial pattern of the ocean evaporation reasonably well in comparison to the OAFlux evaporation data, although in both seasons, both groups of models overestimate evaporation in most latitudes. This overestimation is paricularly prominent from winter to spring (Figure 4.4). Models without ozone depletion tend to overestimate evaporation more than models with ozone depletion. Despite this discrepancy, the overall patterns of evaporation simulated by the models are

again qualititatively similar to those seen in the observations.

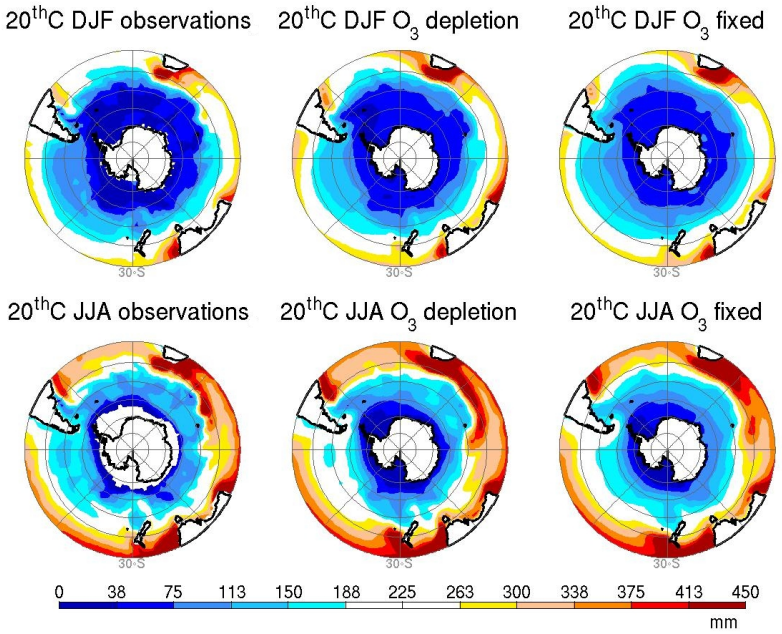

Figure 4.3: Evaporation climatology for 1979–1999. Panels on the left show OAFlux evaporation observations, in the centre show CMIP3 models with ozone depletion and on the right show CMIP3 models without ozone depletion.

Figure 4.4 suggests CMIP3 models have difficulty reproducing the seasonal cycle of evaporation in both high and mid-latitudes. The multimodel averages of both groups are similar, while there is a larger spread in models without ozone depletion. The average of models with ozone depletion is consistently lower and closer to observations than the average of models without ozone depletion for all seasons and in both high and mid-latitudes. However, during September to November the observations lie outside the model spread and the difference is quite considerable, especially in the high latitudes. This suggests that CMIP3 models have systematic biases in ocean latent heat flux in the SH extratropics.

Based on the above assessment it can be concluded that the models reproduce a reasonable evaporation pattern in DJF and JJA, but that evaporation is too high compared to the observations across most of the SH south of 30°S. The models do reproduce a seasonal cycle that is reasonable in summer and autumn but evaporation is too high in winter and spring. Thus the limitations of the models to reproduce adequate evaporation characteristics must be considered when assessing trends in evaporation further in this study.

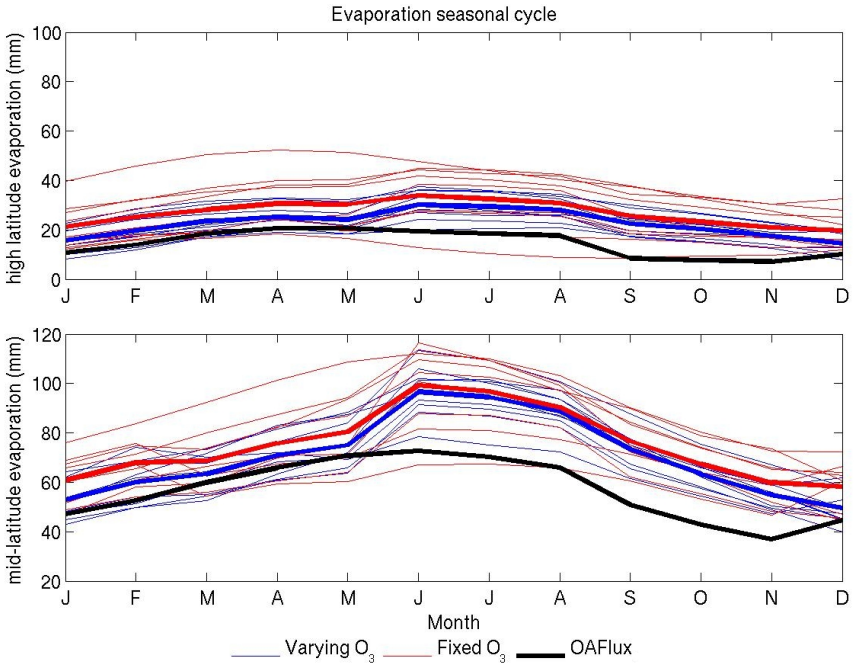

Figure 4.4: Seasonal cycle of zonal-mean evaporation, averaged over 1979–1999 for individual models, multimodel averages and OAFlux evaporation. The top panel shows the seasonal cycle averaged over high latitudes (4–34°S of the jet) and the bottom panel shows the seasonal cycle averaged over mid-latitudes (10–0°N of the jet).

4.1.3 Location of jet

Precipitation patterns are inherently tied to the location of the extratropical eddy-driven westerly jet. However, CMIP3 models show a large variation in their simulations

of the jet (eg. Barnes and Hartmann 2010; Kidston and Gerber 2010). Both the jet location and jet intensity vary significantly among the models as shown in Figure 4.5, which presents the jet location for each model, averaged across the 20C3m and A1B simulations.

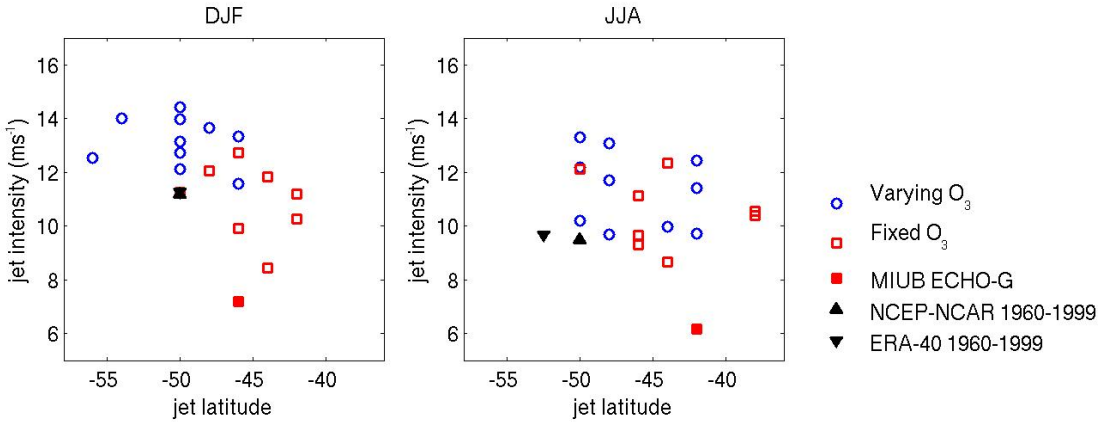

Figure 4.5: Jet intensity versus jet location at 925 hPa. Seasonal-mean jet location and intensity were identified for each century (1960–1999 and 2000–2079) and then averaged to give the values shown. The MIUB ECHO-G jet is shown separately as it was identified using surface wind rather that 925 hPa wind. The locations of the jet in NCEP-NCAR and ERA-40 reanalysis data sets are also shown.

The location of the jet amongst models varies from 42–56°S in DJF and from 38–50°S in JJA. Compared to the reanalysis data, the majority of models lie too far equatorward in DJF and all models lie too far equatorward in JJA (based on the average location of the NCEP-NCAR and ERA-40 jets). Jet intensity also varies amongst models from 8.5–14.4 m s^{-1} in DJF and from 8.7–13.3 m s^{-1} in JJA (excluding the MIUB ECHO-G jet, which is the surface jet rather than 925 hPa jet). Compared to the reanalysis data, the majority of models have jets that are too strong in DJF, although some are too weak. In JJA most models have jets that are too strong.

There is also a separation of the two groups of models in DJF: models with varying ozone forcing have jets that are located further poleward and are more intense than models with fixed ozone forcing. In terms of 20^{th} century jet characteristics this seems reasonable: ozone depletion has been identified as causing a poleward shift and intensification of the jet and thus such separation can be expected. However, the jet characteristics shown are averaged over both the 20^{th} and 21^{st} centuries, so such separation may not be able to be accounted for physically and may indicate a bias in the varying ozone forcing group of models. The lack of obvious separation in the models in JJA, however, suggests that it may not just be model bias. Perhaps the effects of ozone depletion on jet location and intensity in DJF last into the 21^{st} century as almost no trends in the jet are expected in the future because of the cancelling effects of increasing greenhouse gases and ozone recovery.

4.2 Observed trends

As mentioned in Section 3.1, a detailed "quantitative" analysis of the observed trends is not possible due to the nature of the GPCP v2 and OAFlux data sets: merged data sets are constructed with different observations for various time periods and different source data introduces considerable noise in data analysis. Time series of TCO south of 60°S in October, DJF GPCP v2 precipitation and DJF OAFlux evaporation (both in high latitudes) are shown in Figure 4.6. These time series are shown from 1979–2008 during which data from all three data sets is available. A linear trend line is shown on each time series for 1979–1999, the latter part of the twentieth century period analysed for model trends. The TCO time series shows a marked decline in TCO from 1979–1999, followed by ozone levels plateauing from 2000–2008. This is consistent with trends in stratospheric ozone described previously in Section 2.2. Trends in DJF precipitation in high latitudes appear to mirror those in TCO: precipitation increases from 1979–1999 and then appears to plateau.

There is also large interannual variability in both TCO and precipitation and these two data sets show some anticorrelation in interannual peaks. The evaporation shows much less interannual variability and only displays a very weak increasing trend between 1979–1999. This result suggests that trends in precipitation dominate the overall P–E balance and an increasing trend in P–E between 1979–1999 could have contributed to an increased freshwater flux into the Southern Ocean.

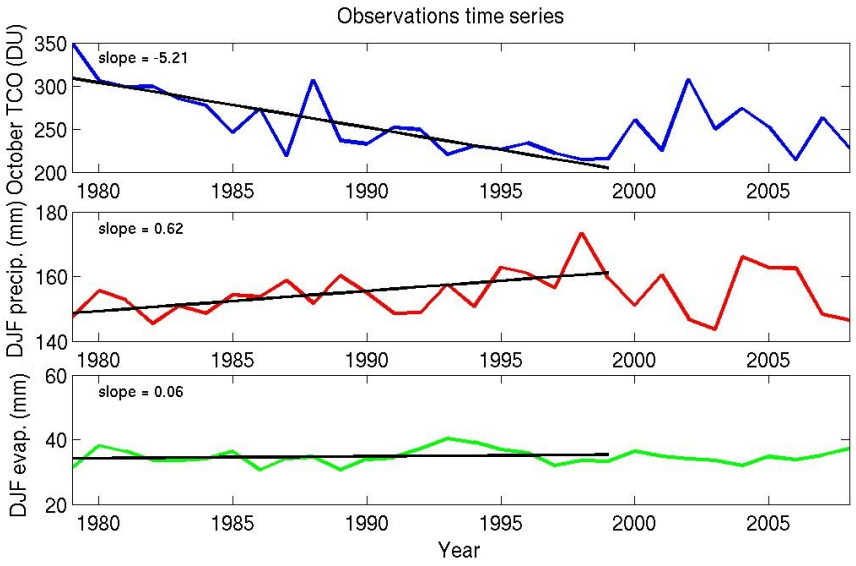

Figure 4.6: Mean ozone, precipitation and evaporation time series for 1979–2008. The top panel shows NIWA mean TCO in October for latitudes south of 60°S, the centre panel shows DJF GPCP v2 precipitation in high latitudes (4–34°S of the NCEP-NCAR jet) and the bottom panel shows DJF OAFlux evaporation in high latitudes (4–34°S of the NCEP-NCAR jet). Trend lines (as determined by a least squares fit) are shown for each variable from 1979–1999.

Figure 4.7 shows time series of DJF and JJA precipitation in high and mid-latitudes between 1960–1999 for models and between 1979–1999 for observations. As with the precipitation seasonal cycle, it can be seen that the multimodel averages of the two groups

of models are similar, but that there is a larger spread in models without ozone depletion. Model spread is also higher in JJA than in DJF. Interannual variability is larger in mid-latitudes than in high latitudes. The multimodel averages are similar to the GPCP v2 precipitation in DJF in high latitudes, which is noteworthy as this is the season and region of primary interest in this study. The multimodel averages are too high with respect to observations in JJA in both high and mid-latitudes and too low in DJF in mid-latitudes.

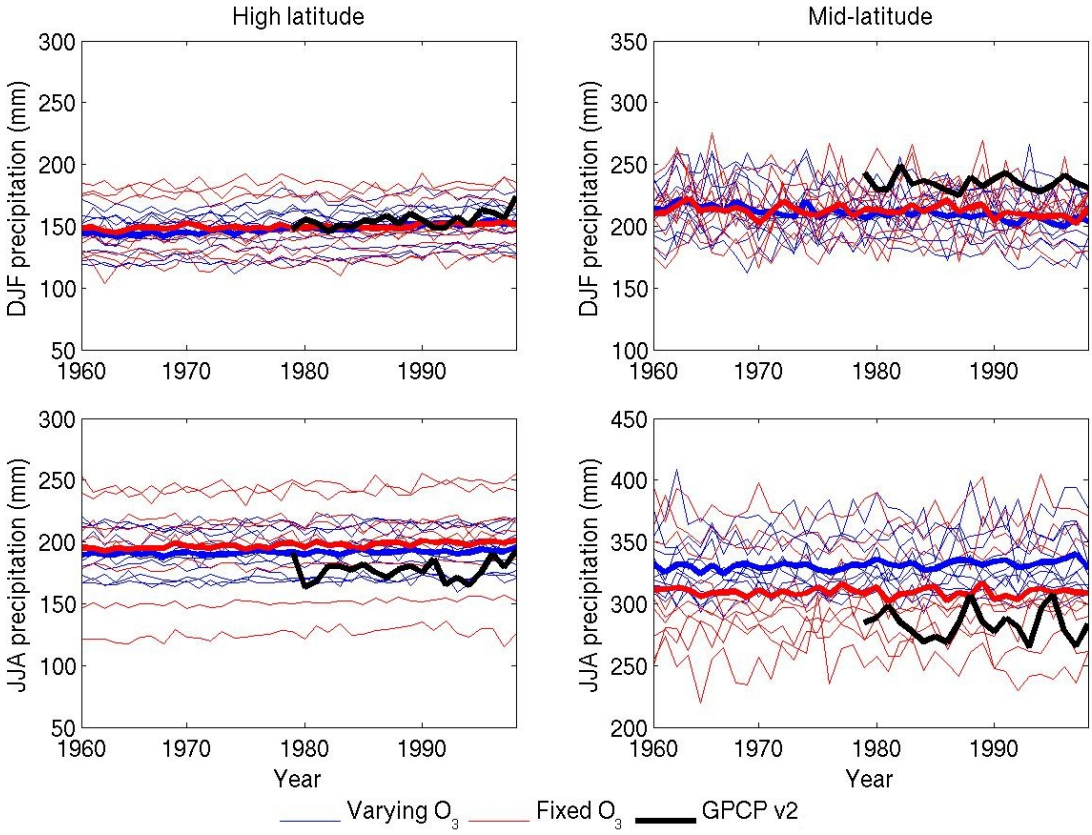

Figure 4.7: Seasonal-mean precipitation time series for 1960–1999 for individual models, multimodel averages (shown in bold) and GPCP v2 precipitation (shown only from 1979–1999 due to data availability). Panels on the left are averaged over high latitudes (4–34°S of the jet) and panels on the right are averaged over mid-latitudes (10–0°N of the jet). The top panels show DJF precipitation and the bottom panels show JJA precipitation.

It is difficult to describe in detail the model trends in Figure 4.7 due to the large number of models shown. In DJF it can be seen that the multimodel-mean precipitation in high latitudes of models with ozone depletion increases more rapidly over the time period 1960–1999 than the multimodel average of models without ozone depletion. In JJA the reverse is true, although less visible. Precipitation trends in mid-latitudes are more noisy and it is difficult to draw any conclusions at this point.

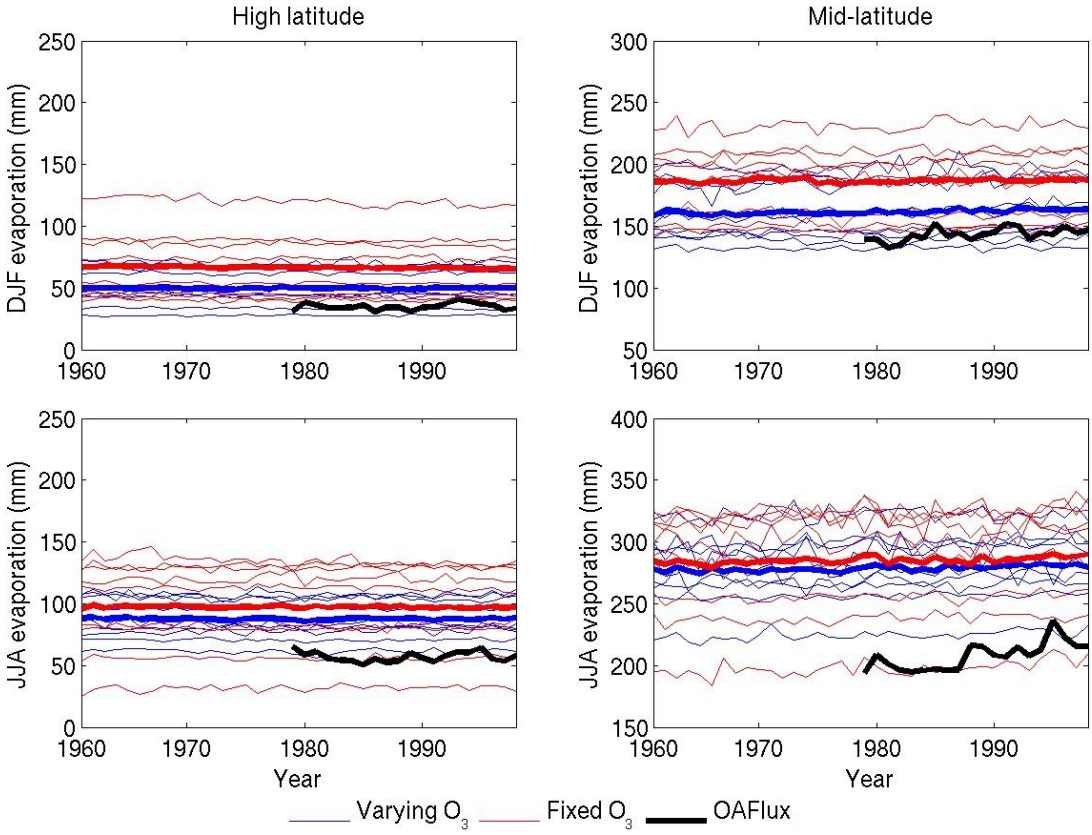

Figure 4.8: Seasonal-mean evaporation time series for 1960–1999 for individual models, multimodel averages (shown in bold) and OAFlux evaporation (shown only from 1979–1999 due to data availability). Panels on the left are averaged over high latitudes (4–34°S of the jet) and panels on the right are averaged over mid-latitudes (10–0°N of the jet). The top panels show DJF evaporation and the bottom panels shows JJA evaporation.

As described in Section 4.1.2, the models consistently overestimate evaporation in both high and mid-latitudes and in both DJF and JJA (Figure 4.8). The models without ozone depletion have consistently higher evaporation than the models with ozone depletion, although the reason for this remains to be determined. Again the models without ozone depletion show a larger spread. The model-simulated trends in evaporation appear almost negligible for all seasons and latitudes.

4.3 Model simulated trends: monthly-mean data

The previous section presented preliminary results of the trends simulated by CMIP3 models. Next, the multimodel-mean trends across the extent of the SH south of 30°S are presented to identify the geographic distribution of precipitation and evaporation trends and to compare the trends of models with varying ozone forcing and those with fixed ozone forcing.

For all multimodel trend figures, top panels show SH summer (DJF) trends and bottom panels show SH winter (JJA) trends. From left to right, trends are shown for models with and without ozone depletion in the 20^{th} century and for models with and without ozone recovery in the 21^{st} century respectively. As detailed in Chapter 3, trends are determined by least squares fit for individual models and mean trends are calculated by linearly interpolating each model's trend to a standard grid and then averaging across all models in a group. All trends shown are seasonally accumulated trends. Cool colours denote an increasing freshwater flux (increasing precipitation trend or decreasing evaporation trend) whilst warm colours denote a decreasing freshwater flux (decreasing precipitation trend or increasing evaporation trend). Hatched areas denote where the multimodel mean trend is greater than or equal to one standard deviation of the trends of different models within

that group.

4.3.1 Precipitation (P)

Multimodel trends in precipitation derived from monthly-mean data are shown in Figure 4.9. This figure shows that in 20^{th} century DJF, models with ozone depletion exhibit a much stronger dipole trend in precipitation than models without ozone depletion. Models with ozone depletion have a strong increasing trend in high latitudes around Antarctica (between approximately 50–75°S) and a strong decreasing trend in mid-latitudes (between approximately 40–50°S). Models without ozone depletion exhibit a weak increasing trend in high latitudes around Antarctica. These findings are consistent with the previous studies presented in Section 2.3: increasing greenhouse gases cause a poleward shift in the extratropical westerly jet, moving storm tracks poleward, explaining the trends in the multimodel average of models with fixed ozone. Ozone depletion also causes a poleward movement of storm tracks and the combination of ozone forcing and greenhouse gas forcing in the models with ozone depletion leads to much stronger trends being observed in this multimodel average. The high latitude results are supported by the comparison with observations in Section 4.1.1 concluding that the models simulated the high latitude climate between 1979–1999 well in DJF.

In 20^{th} century JJA the multimodel averages of the two groups of models are more similar. There is an increasing trend in high latitudes and a decreasing trend around 30–40°S. Trends in the models without ozone depletion are more pronounced compared to the models with ozone depletion. In this case, the general trends are again consistent with the previous studies presented in Section 2.3: ozone depletion has no influence during SH winter so both sets of models display changes due only to greenhouse gas forcing. This

results in the two groups of models being more similar and displaying a weak increase in precipitation in high latitudes and a weak decrease in precipitation in mid-latitudes. The differences between the two sets of models in JJA is attributed to intermodel differences and model biases. Additionally, it should be noted that when models are compared with observations in Section 4.1.1, notable differences are seen between multimodel averages and observations in both high and mid-latitudes between 1979–1999 in JJA, suggesting that the models do not simulate winter climate as well as they do summer climate, which may contribute to intermodel differences in this season.

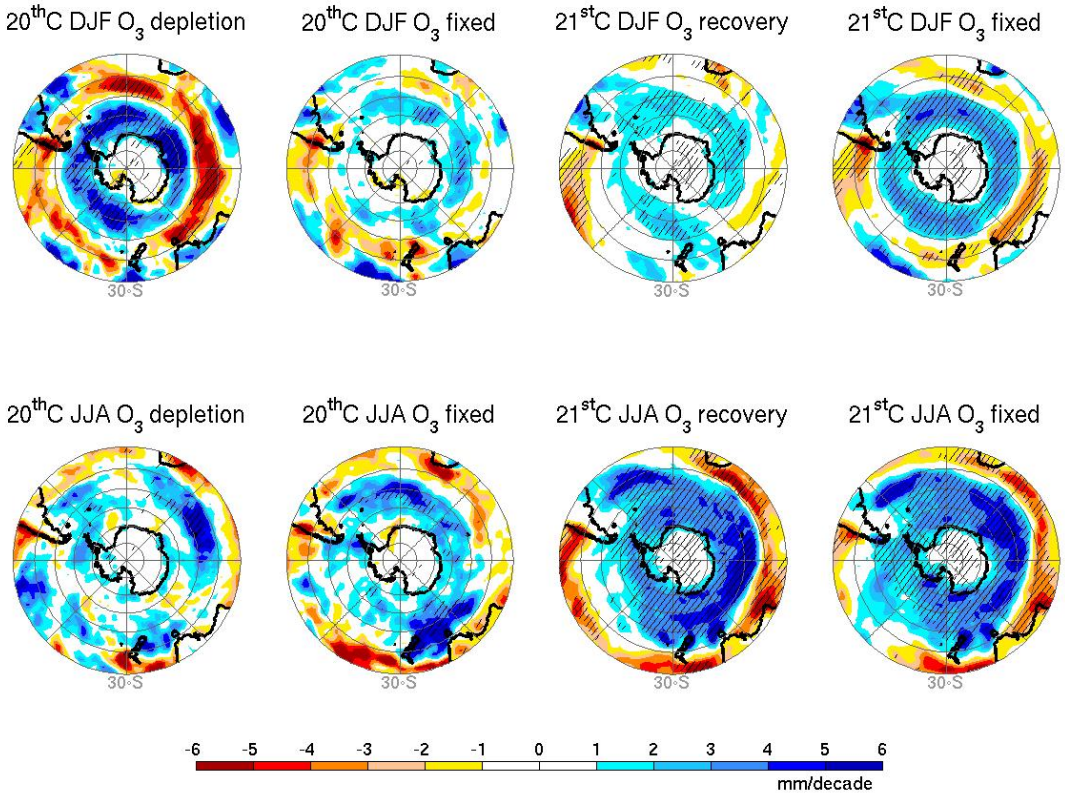

Figure 4.9: Multimodel-mean trends in seasonal precipitation for the four model groups.

In 21^{st} century DJF the models with ozone recovery display much weaker trends than the models with fixed ozone forcing. Both sets of models show an increasing trend in precipitation in high latitudes (between approximately 50–70°S) and a decreasing trend in mid-latitudes (between approximately 35–50°S). Compared to the magnitude of trends in the 20^{th} century, 21^{st} century trends are generally stronger than those of models with fixed ozone forcing in DJF, but weaker than those of models with ozone depletion in DJF. Once again this is as expected from the previous studies presented in Section 2.3: greenhouse gases continue to increase in the 21^{st} century, leading to stronger trends in precipitation (models with fixed ozone forcing), however ozone recovery counteracts some of the greenhouse gas effects, leading to weaker trends in precipitation in those models that incorporate both greenhouse gas forcing and ozone recovery (models with varying ozone forcing). In 21^{st} century JJA the two sets of models appear very similar, with similar increasing precipitation poleward of approximately 40°S and decreasing precipitation between 30–40°S. This suggests that intermodel differences in the 21^{st} century are smaller and allows differences in DJF to be more conclusively attributed to ozone forcing.

It is worthwhile noting that the findings of the precipitation trend analysis are consistent with those of Son et al. (2009) despite a different set of CMIP3 models being used in their study. This suggests that the results are robust and are not dependent on the specific models used in each model group.

Figure 4.5 shows that there is a large spread in the location of the extratropical westerly jet amongst models. Motivated by this fact, Figure 4.10 shows the DJF zonal-mean precipitation climatologies and trends for individual models and multimodel averages versus

absolute latitude and versus latitude relative to the jet. Zonal-mean GPCP v2 precipitation is also shown on the precipitation climatology panels for reference. It is evident that, although qualitatively similar, the models do not capture the meridional variation in precipitation very well: models do not simulate the double-peak in precipitation that the GPCP v2 data does and they underestimate precipitation around 60°S and around 30–40°S.

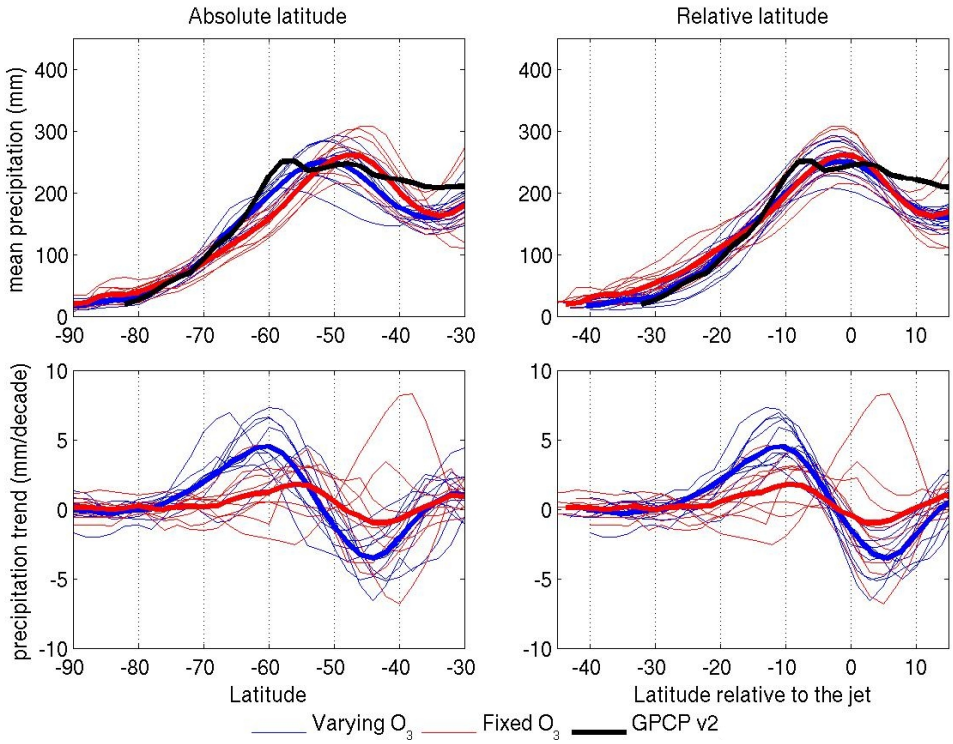

Figure 4.10: Zonal-mean DJF precipitation versus absolute latitude (left) and versus latitude relative to the jet (right). The top panels show climatological precipitation and the bottom panels show precipitation trend for the individual models. Zonal-means are shown for individual models, multimodel averages (bold) and observations (bold black).

Figure 4.10 also shows that the peak in zonal-mean precipitation varies amongst models, but when precipitation is plotted versus latitude relative to the jet, precipitation peaks

align more closely. The same can be seen in the trend panels. This demonstrates that precipitation patterns are dependent on jet location and thus justifies the decision to tailor statistical tests to models based on their individual jet locations.

4.3.2 Evaporation (E)

Multimodel trends in evaporation derived from monthly-mean data are shown in Figure 4.11. In contrast to the clearly defined annular trends seen in precipitation (Figure 4.9), trends in evaporation are much less zonally coherent and are of much weaker magnitude than those of precipitation. This finding is somewhat unexpected: it was in fact expected that the changes in surface winds attributed to ozone forcing would lead to coherent trends in ocean evaporation, however this is not the case. Differences can be seen between models with varying ozone and models with fixed ozone in both centuries and both seasons, but they lack structure and are very noisy. Additionally, as is noted in Section 4.1.2, both groups of models are found to have considerable differences compared to the OAFlux evaporation. Hence, attribution of trends to ozone forcing versus greenhouse gas forcing is not possible or particularly meaningful in the evaporation field.

4.3.3 Precipitation minus evaporation (P–E)

Multimodel-mean trends in P–E derived from monthly-mean data are shown in Figure 4.12. Trends in P–E are very similar to those in precipitation, which is expected as trends in precipitation are much larger and more defined than those in evaporation (Section 4.3.2). Thus it is evident that, consistent with observations, model trends in precipitation dominate the overall P–E balance in the SH south of 30°S and from this it can be concluded that stratospheric ozone changes influence the hydrological cycle in the SH summer primarily

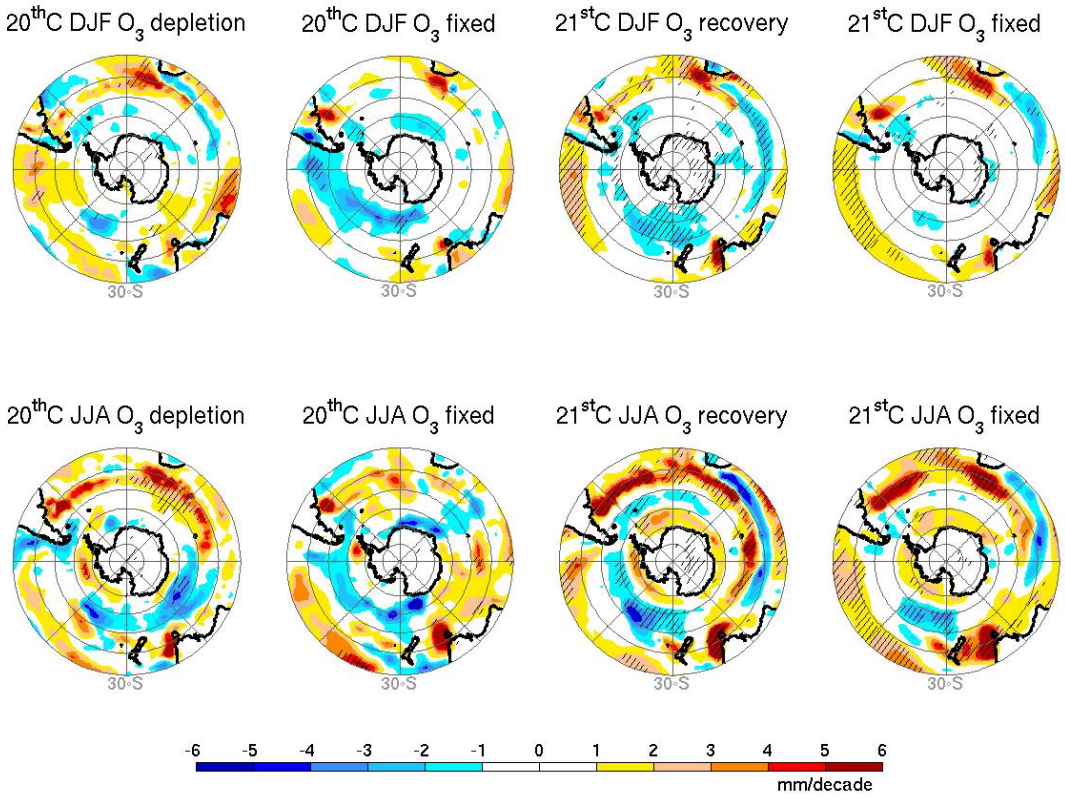

Figure 4.11: Multimodel-mean trends in seasonal evaporation for the four model groups.

through changes in precipitation.

4.4 Model simulated trends: daily-mean data

To gain better understanding into the impact of stratospheric ozone changes on the SH hydrological cycle, it is desirable to examine changes in the intensity and frequency of precipitation events. Evaporation is not examined in further detail as it is found to be less important than precipitation in trends in P–E. Information on the intensification and frequency of precipitation events cannot be obtained from monthly-mean data, so daily-mean data is required for this analysis. As daily-mean data is not available continuously in the

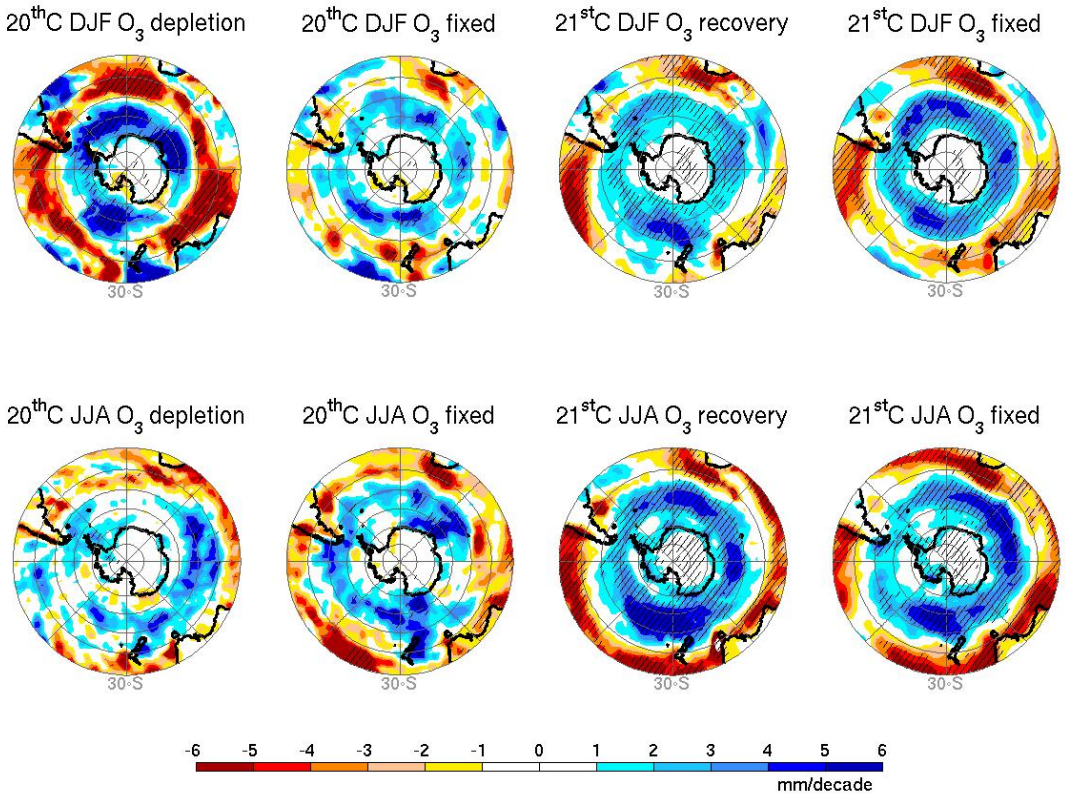

Figure 4.12: Multimodel-mean trends in seasonal P–E for the four model groups.

21^{st} century, trend detection via the decadal-difference method is necessitated.

4.4.1 Decadal-difference precipitation

Multimodel trends in precipitation derived from daily-mean data using the decadal-difference method are shown in Figure 4.13. These trends are very similar to those found using monthly-mean data and linear regression (Figure 4.9) demonstrating that the decadal-difference method is suitable for trend detection. However, the magnitude of trends are weaker than those in Figure 4.9, particularly in the 21^{st} century, suggesting that the decadal-difference method is less sensitive to trend detection than linear regression. It

is not unexpected that the trends in the 21^{st} century are the most affected, as the 1990s are used in calculating 21^{st} century trends, so trends in models with varying ozone forcing are likely to be subdued as this takes into account decades during both the ozone depletion and recovery phases and some signals may be cancelled out. The overall similarity between the two trend detection methods, however, allows the conclusions drawn from the monthly-mean analysis to be applied to the daily analysis.

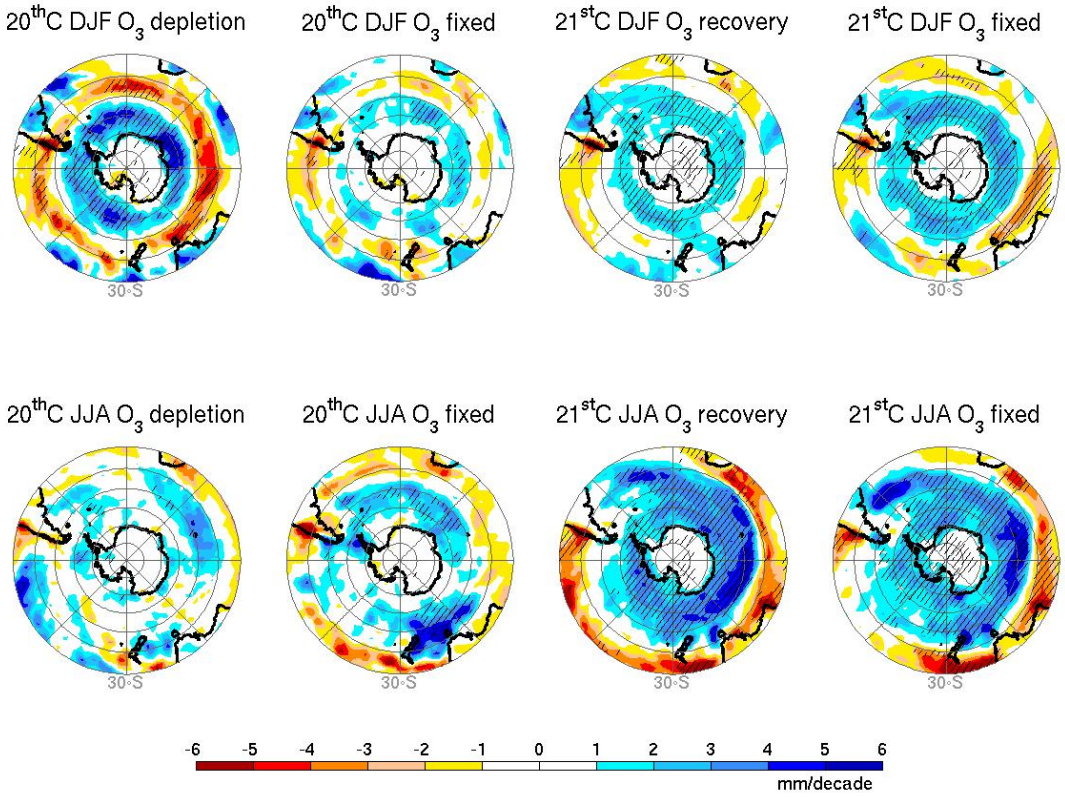

Figure 4.13: Multimodel-mean trends in seasonal precipitation calculated using daily-mean data for the four model groups. 20^{th} and 21^{st} century trends were calculated by differencing 1961–1970 from 1990–1999, and 1990–1999 from 2056–2065, respectively.

4.4.2 Precipitation intervals

To understand precipitation decadal-differences shown in Figure 4.13 in depth, precipitation at different intensities is further examined. Multimodel trends in very light, light and moderate to heavy precipitation regimes are shown in Figure 4.14, Figure 4.15 and Figure 4.16 respectively. For each of these figures, the top panel shows trends in the frequency of precipitation in that regime and the bottom panel shows trends in the total accumulation of precipitation in that regime.

For the very light (0.1–1 mm day^{-1}) precipitation regime it can be seen that trends in the frequency of precipitation (Figure 4.14A) are actually in the opposite sense to trends in mean precipitation. That is, there is a decrease in the frequency of very light precipitation in high latitudes and an increase in very light precipitation in mid-latitudes. Trends are most pronounced in the 20^{th} century DJF models with ozone depletion, however they are still evident in other seasons and centuries. The differences between models with varying ozone forcing and models with fixed ozone forcing discussed previously apply here in the opposite sense. The physical cause of these trends is unknown, however results are consistent with the findings by Sun et al. (2007), where very light precipitation was found to decrease around 65°S in global warming simulations. Although the changes in the frequency of very light precipitation are somewhat surprising, these precipitation events contribute only a very small fraction to total precipitation amount. Figure 4.14B shows that the trends in accumulation of very light precipitation are negligible. The colour scale in this panel is chosen to be consistent with the colour scale in Figure 4.15B and Figure 4.16B and demonstrates that changes in this precipitation regime have little impact on changes in the mean. Refer to Appendix A (Figure A.1) for the same figure with an altered colour scale.

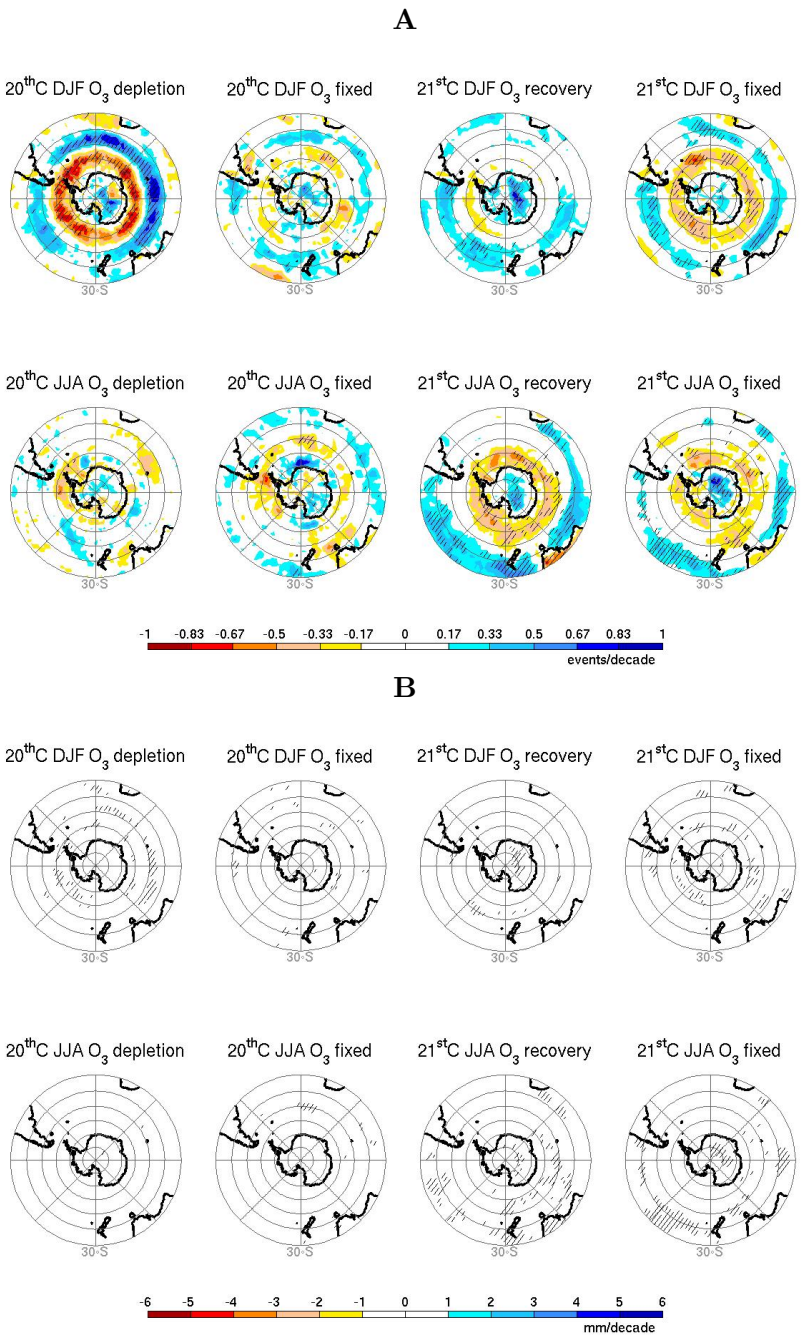

Figure 4.14: Multimodel-mean trends in the frequency and accumulation of daily precipitation events for the 0.1–1 mm day^{-1} regime (**A** shows frequency and **B** shows accumulation) for the four model groups. The colour scale in **B** is consistent with that of Figure 4.15B and Figure 4.16B: the absence of shading indicates this regime has a negligible contribution to mean precipitation.

For the light (1–10 mm day^{-1}) precipitation regime it can be seen that trends in the frequency (Figure 4.15A) and accumulation (Figure 4.15B) are very similar to trends in mean precipitation (Figure 4.13), although light precipitation trends are generally weaker than trends in mean precipitation. This finding is also consistent with the findings by Sun et al. (2007): as light precipitation makes up a large contribution of total precipitation (too large a proportion compared to observations), under global warming conditions, changes in total precipitation were reflected in changes in light precipitation.

For the moderate to heavy (>10 mm day^{-1}) precipitation regime the trends in the frequency (Figure 4.16A) are small, however as a small change in the number of moderate to heavy events has a more significant effect on total precipitation, larger trends are seen in the accumulation (Figure 4.16B). Trends in accumulation are predominantly increasing across the SH, indicating that moderate to heavy precipitation events are increasing, however there are no notable differences between models with varying ozone forcing and models with fixed ozone forcing, indicating that stratospheric ozone changes have little effect on moderate to heavy precipitation. This is discussed further in Section 4.4.3.

In summary the trends in frequency and accumulation of different precipitation intensities suggest that trends in mean precipitation attributed to varying ozone forcing are mostly due to trends in the light precipitation regime. Trends in the very light precipitation regime are opposite in sign to those of the light precipitation regime, however this regime contributes very little to total precipitation. Trends in moderate to heavy precipitation are similar in models with varying ozone and fixed ozone forcing, so it is likely that this precipitation regime is not affected by varying ozone forcing.

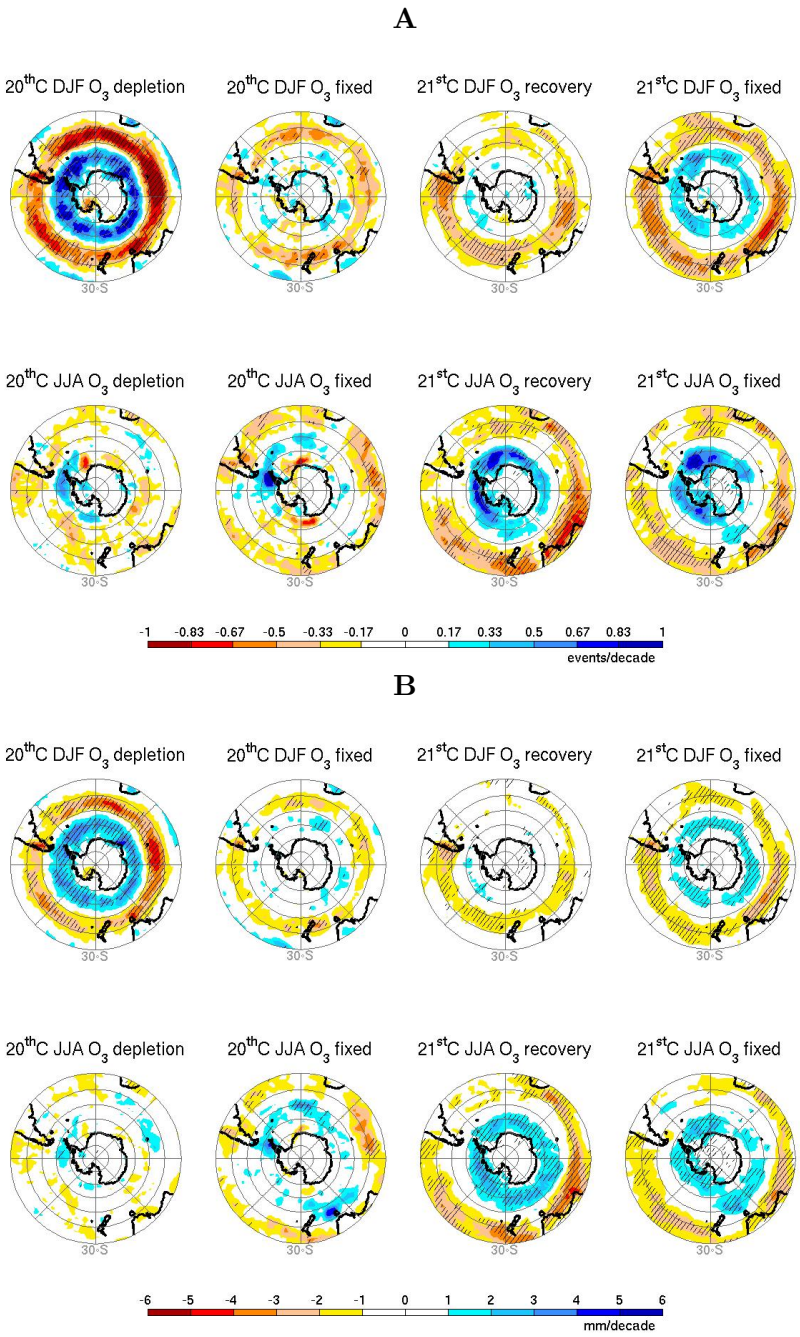

Figure 4.15: Multimodel-mean trends in the frequency and accumulation of daily precipitation events for the 1–10 mm day^{-1} regime (**A** shows frequency and **B** shows accumulation) for the four model groups.

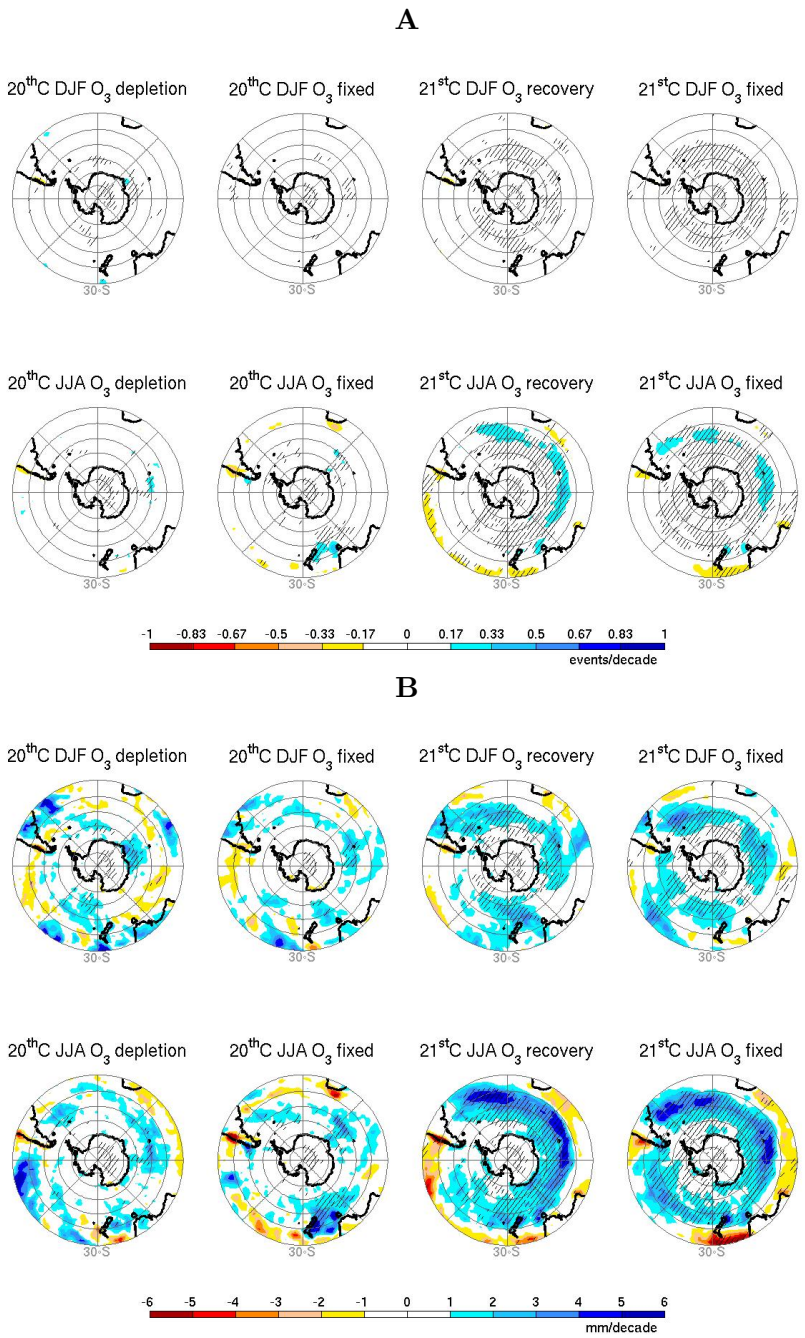

Figure 4.16: Multimodel-mean trends in the frequency and accumulation of daily precipitation events for the >10 mm day^{-1} regime (**A** shows frequency and **B** shows accumulation) for the four model groups. The colour scale in **A** is consistent with that of Figure 4.14A and Figure 4.15A: little shading indicates little change in the frequency of moderate to heavy events.

In review of the magnitude of trends in light precipitation frequency (Figure 4.15A), it can be seen that 20^{th} century DJF trends in high latitudes for models with ozone depletion are only of the order of 1 event decade^{-1}. Although this seems small, an increase of one 2–5 mm precipitation event (found to be the most common intensity within the 1–10 mm day^{-1} regime) provides the observed increase in mean precipitation (Figure 4.13) due to accumulation of light precipitation events (Figure 4.15B). Again, this increase in precipitation accumulation, attributable to ozone depletion, may seem small. Over a 40-year period, however, a 4 mm decade^{-1} increase in precipitation amounts to an increase of 16 mm. Given that DJF precipitation in high latitudes is ∼150–200 mm (Figure 4.2, Figure 4.7 and Figure 4.10), this corresponds to an increase of approximately 10 %, which is considerable.

4.4.3 Extreme precipitation

Multimodel trends in the simple precipitation index are shown in Figure 4.17. Each map in this figure is predominantly blue, indicating an intensification of precipitation intensity, consistent with greenhouse gas forced warming (eg. Emori and Brown 2005; O'Gorman and Schneider 2009). There are no notable differences between models with varying ozone forcing and models with fixed ozone forcing in either century or season.

Results appear similar to those seen in Figure 4.16, indicating that precipitation intensities of >10 mm day^{-1} approximate extreme precipitation events in the SH extratropics (and hereinafter are grouped with extreme precipition indices). Similar results are found for other extreme indices, shown in the Appendix (Figure A.3 and Figure A.4). These findings suggest that stratospheric ozone changes do not affect extreme precipitation.

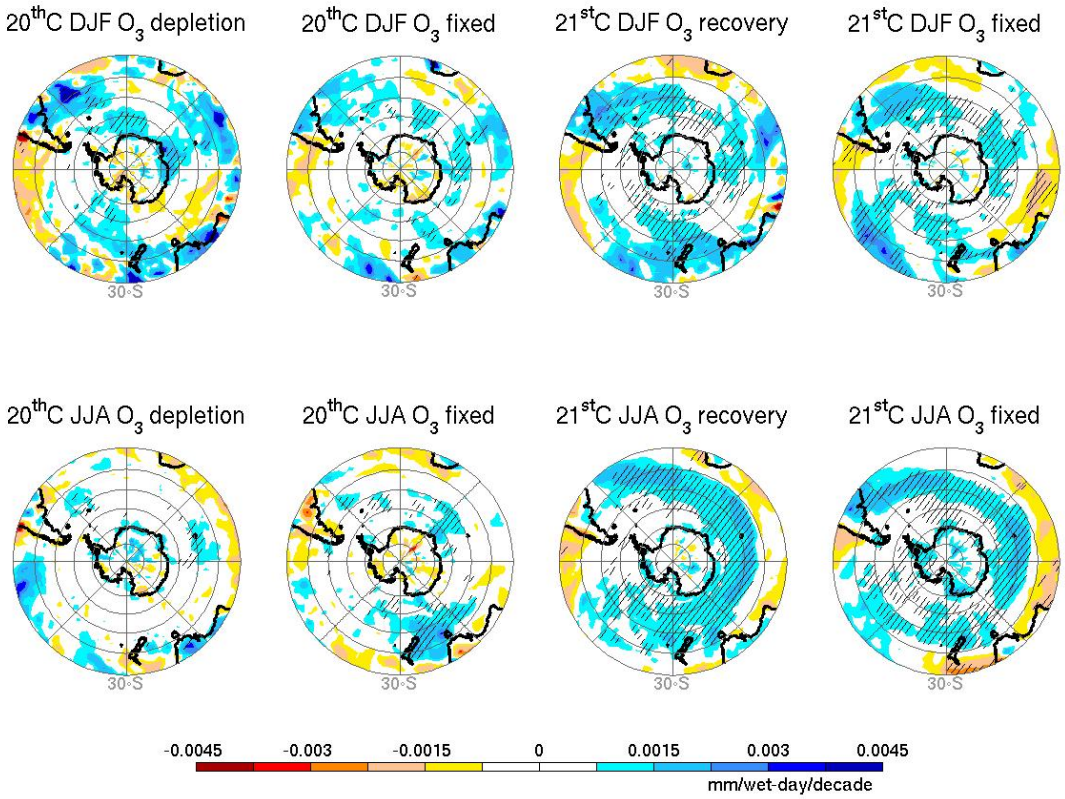

Figure 4.17: Multimodel-mean trends in the simple precipitation index for the four model groups.

This result is consistent with the findings of previous studies. As discussed in Section 2.4.3, Emori and Brown (2005) separated climate change components that affect precipitation extremes into dynamic effects, such as changes in vertical motion, and thermodynamic effects, such as changes in saturation water vapour pressure as the climate warms. Stratospheric ozone changes affect mean precipitation by inducing a poleward shift and intensification of the extratropical westerly jet: that is, stratospheric ozone changes affect mean precipitation via dynamic effects. Here trends in vertical motion at 500 hPa are examined (refer to Figure A.2 in the Appendix) and are found to be consistent with the trends in

mean precipitation, confirming that stratospheric ozone affects precipitation dynamically. On the other hand, stratospheric ozone changes have previously been shown to have little impact on surface air temperature (eg. Son et al. 2009), which controls saturation water vapour pressure (refer to Figure A.2 in the Appendix).

Findings by Emori and Brown (2005), O'Gorman and Schneider (2009) and Gastineau and Soden (2009) suggest that in the extratropics the influence of dynamic effects on extreme precipitation was almost negligible and that changes in extreme precipitation were due almost entirely to changes in thermodynamic effects. Because stratospheric ozone changes do not induce thermodynamic changes in most of the SH extratropical troposphere then it follows that extreme precipitation is not affected by stratospheric ozone forcing. Thus the results of trends in extreme precipitation presented here agree with the theory presented by Emori and Brown (2005), O'Gorman and Schneider (2009) and Gastineau and Soden (2009)

4.5 Statistical significance

The discussion of differences between the multimodel-means of the two groups of models so far has been based only on a visual assessment of figures. Here a discussion of the findings of statistical significance tests are presented, with results of the statistical comparison between models with varying ozone forcing and models with fixed ozone forcing summarised in Table 4.1 and Table 4.2. Significance tests were applied to all CMIP3 models used in this study to obtain the results presented.

Table 4.1 summarises results for the high latitude (4–34°S of the jet) region. From this table it can be seen that in both centuries the two groups of models are found to be

significantly different during DJF for all precipitation measures except extreme precipitation indicators and surface air temperature. These results support the findings presented above and suggest that stratospheric ozone changes have a significant influence on the mean hydrological cycle in high latitudes during SH summer.

Table 4.1: Summary of statistical significance in trend differences between the models with varying ozone forcing and the models with fixed ozone forcing for the high latitude region. Statistical significance is assessed with a t-test and a Monte Carlo approach. Significance is found at the same levels, except for the italicised text which was calculated as shown with a t-test and one level of significance higher with the Monte Carlo approach. Minus (–) (plus (+)) indicates the multimodel-mean trend of the varying ozone forcing models is less (more) than that of the fixed ozone forcing models. All seasons are shown for both centuries: empty columns are included as they signify no differences between the two groups of models in the corresponding season.

	20C3m Significant Difference				**A1B Significant Difference**			
Variable	**DJF**	**MAM**	**JJA**	**SON**	**DJF**	**MAM**	**JJA**	**SON**
Precipitation	+ 99.9%		– 95%		– 99%			
Evaporation	*+ 95%*				– 95%			
P–E	+ 95%		– 95%		– 95%			
Daily precip.	+ 99.9%				– 95%			
SDII								
R95pTOT								
R99pTOT								
Rx1day								
Rx5day								
F0.1–1 mm day^{-1}	– 99%				+ 99.9%			
F1–10 mm day^{-1}	+ 99.9%				– 95%			
F>10 mm day^{-1}								
A0.1–1 mm day^{-1}	– 95%				+ 99%			
A1–10 mm day^{-1}	+ 99.9%				– 95%			
A>10 mm day^{-1}								
Surface temp.								
500 hPa omega	– 95%		+ 95%		+ 95%			

As no significant difference is found for any extreme precipitation indicators or surface temperature, this supports the argument made in Section 4.4.3. Thus, there is confidence that stratospheric ozone changes have negligible impact on extreme precipitation because thermodynamic effects control extreme precipitation in the extratropics and stratospheric

ozone does not cause any significant trends in thermodynamic effects, which are largely controlled by surface air temperature in the regions of interest.

Table 4.2: Summary of statistical significance in trend differences found between models in mid-latitudes: results are shown as for Table 4.1.

	20C3m Significant Difference				**A1B Significant Difference**			
Variable	**DJF**	**MAM**	**JJA**	**SON**	**DJF**	**MAM**	**JJA**	**SON**
Precipitation	– 95%		+ 95%		+ 99%	+ 99%		
Evaporation					– 95%	– 95%		– 95%
P–E			+ 95%		+ 99.9%	*+ 99%*		
Daily precip.	– 95%					*+ 95%*		
SDII								
R95pTOT								
R99pTOT				– 95%				
Rx1day								
Rx5day					– 95%			
F0.1–1 mm day^{-1}	+ 95%							
F1–10 mm day^{-1}	*– 99%*							
F>10 mm day^{-1}			+ 95%			+ 95%		
A0.1–1 mm day^{-1}								
A1–10 mm day^{-1}	*– 95%*							
A>10 mm day^{-1}			+ 95%			+ 95%		
Surface temp.								
500 hPa omega			– 95%			– 95%		

Table 4.1 also shows significant differences during JJA in the 20^{th} century for precipitation (monthly-mean), P–E (a manifestation of the significance found in precipitation) and 500 hPa omega. This could be problematic as it suggests that differences attributed to stratospheric ozone forcing in DJF may actually be due, at least in part, to intermodel differences, as the influence of ozone in JJA is negligible. However, because models exhibit a larger spread in JJA precipitation suggesting models simulate winter conditions more poorly than summer conditions, there is less confidence in the JJA statistical results than there is in DJF results. Additionally, significance is found only at the 95 % confidence level in JJA, whereas it is found at higher confidence levels in many cases in DJF. Finally the significance in JJA is in the opposite sense to that in DJF: in JJA models without ozone

depletion exhibit a larger positive trend in precipitation in high latitudes, whereas in DJF models with ozone depletion exhibit the larger positive trend. This means that although it is likely some model bias has affected results, the models with ozone depletion are actually biased towards lower precipitation trends in JJA and so the strong increasing precipitation trends that they exhibit during DJF can still be attributed to stratospheric ozone decline.

Table 4.2 summarises results for the mid-latitude (10–0°N of the jet) region. At first glance it is evident that much less consistent results are found for this region than for the high latitude region. This is likely caused, at least in part, by the higher variability in both precipitation and evaporation (refer to Figure 4.7 and Figure 4.8) in the mid-latitudes.

In 20^{th} century DJF significant differences are found in mean precipitation but not in mean evaporation or P–E. Significant differences are also only found in some of the precipitation regime measures. In 21^{st} century DJF significant differences are found in precipitation trend assessed with monthly-mean data and linear regression, but not in precipitation assessed with daily data and the decadal-difference method, indicating mean precipitation trends in mid-latitudes in the 21^{st} century are less robust than in the 20^{th} century. The lack of significant differences in DJF suggests that the influence that stratospheric ozone forcing has during SH summer in mid-latitudes is less pronounced than in high latitudes.

More comprehensive significance is found in 21^{st} century MAM. The reason for this is unknown, however the asymmetric behaviour of stratospheric ozone changes may play a role: as stratospheric ozone recovery is expected to cause stratospheric temperature anomalies one month later than those associated with stratospheric ozone decline (Son

et al. 2010), tropospheric effects may also be delayed and this may result in ozone induced changes being detected in MAM.

Significance is also found during other seasons (JJA in the 20^{th} century and SON in both centuries) and for some extreme precipitation measures. The reasons for this are unknown and differences are likely attributed to intermodel differences and biases. It should be noted however, that significance for both the frequency and accumulation of moderate to heavy precipitation in 20^{th} century JJA and 21^{st} century MAM are not considered to be indicative of extreme precipitation in this latitude, but rather of changes in mean precipitation in regions where heavier precipitation events are more common.

The findings of the statistical analysis for mid-latitudes are much less conclusive than those for high latitude results. Stratospheric ozone forcing may have some influence on mid-latitude hydrology, as statistical differences are present between the two groups of models for a number of measures in DJF, however significance is also found during other seasons as well as for measures such as extreme precipitation that stratospheric ozone changes have been argued above to have little impact on. Thus it is difficult to attribute differences to stratospheric ozone forcing as in the mid-latitudes intermodel differences are considerable.

Despite this, alternate analysis (refer to Section 5.3) could yield more conclusive significance for the mid-latitude region. That significance for the high latitude region is found, combined with the theory of how ozone-induced changes to tropospheric dynamics affect both high and mid-latitude regions suggests that hydrological changes in the mid-latitude region may still be discerned with further investigation.

In summary, these statistical tests suggest that in high latitudes stratospheric ozone changes have a significant impact on SH summer precipitation, evaporation and P–E. In the 20^{th} century stratospheric ozone depletion increases the positive trend in P–E relative to only greenhouse gas forcing, thus increasing the freshwater flux into the Southern Ocean. In the 21^{st} century stratospheric ozone recovery reduces the positive trend in P–E relative to only greenhouse gas forcing, thus minimising freshwater flux into the Southern Ocean. Although some differences between the groups of models in 20^{th} century JJA are also found to be significant, as reasoned above, this finding does not undermine conclusions about the influence of stratospheric ozone changes on high latitude climates in the SH summer.

Chapter 5
Conclusions

5.1 Summary

The purpose of this research is, building on the findings of Son et al. (2009), to conduct a multimodel study using output from CMIP3 models to investigate in further detail the influence of stratospheric ozone changes on SH hydrological changes. Monthly-mean precipitation and evaporation data are analysed and precipitation is found to dominate overall changes in the P–E balance. Daily-mean precipitation data are also used to investigate the trends in mean precipitation further: trends in very light, light and moderate to heavy precipitation frequencies and accumulations are examined, as are trends in a variety of extreme precipitation indices.

Stratospheric ozone is found to have a statistically significant impact on mean summer precipitation in high latitudes and this effect is primarily through changes in the light (1–10 mm day^{-1}) precipitation regime. During the 20^{th} century, stratospheric ozone depletion resulted in a stronger increasing trend in precipitation in high latitudes then due to greenhouse gas forcing alone. During the 21^{st} century, stratospheric ozone recovery resulted in a weaker increasing trend in precipitation in high latitudes compared to the influence of greenhouse gas forcing alone. This result has an important implication to the freshwater flux into the Southern Ocean as discussed below in Section 5.2.

Results of the influence of stratospheric ozone forcing in mid-latitudes are less conclusive. Qualitatively, trend maps show that in 20^{th} century DJF ozone depletion strengthened the decreasing precipitation trend in mid-latitudes. During 21^{st} century DJF, as ozone is predicted to recover, the impact is seen to be the opposite. Statistical significance tests for the mid-latitude trends are however, much less consistent than for the high latitude trends. Thus findings suggest ozone forcing could play a role at these latitudes but higher interannual variability and intermodel differences may obscure the trends.

Ozone forcing is not found to affect extreme precipitation, consistent with arguments presented by Emori and Brown (2005) and O'Gorman and Schneider (2009): in the extratropics thermodynamic effects control extreme precipitation changes, however ozone forcing alters seasonal mean precipitation through dynamic effects and has little thermodynamic impact. Thus no changes in extreme precipitation would be expected as a result of stratospheric ozone changes.

In summary, the results of this study show that stratospheric ozone forcing affects SH summer-mean precipitation but not extreme precipitation. The influence of ozone forcing during SH summer is qualitatively evident in both high and mid-latitudes, however is significant only in high latitudes. The influence of stratospheric ozone trends is evident in model simulations from both the 20C3m and A1B simuluations, however trends in the 20^{th} century during the ozone depletion phase are the most pronounced.

5.2 Implications to the Southern Ocean

Observations from the latter half of the 20^{th} century show changes in a number of the Southern Ocean characteristics including temperature, salinity and circulation. Warming

has occurred over much of the extent of the Southern Ocean, extending to depths of up to 1,200m in the Antarctic Circumpolar Current (ACC) (Wong et al. 1999; Gille 2002, 2003; Aoki et al. 2003; Levitus et al. 2005; Jacobs 2006; Böning et al. 2008; Forster et al. 2010). Surface freshening has been observed over the entire latitudinal extent of the ACC (Böning et al. 2008) as well as at depths further north in Antarctic intermediate water signatures (Wong et al. 1999; Boyer et al. 2005). The ACC has also been observed to accelerate eastwards and shift poleward (Jacobs 2006; Böning et al. 2008; Toggweiler and Russell 2008; Forster et al. 2010) consistent with the changes in surface winds.

Changes to the Southern Ocean are significant, not just in themselves, but also because the Southern Ocean is an important heat and carbon sink and thus regulates global climates. The importance of the Southern Ocean on global climates depends on the strength of the ACC and the fluxes that mix subtropical waters into and across it (Gille 2002, Gille 2003). Changes in the carbon uptake of the Southern Ocean as well as in deep ocean circulation have already been observed and are predicted to continue in the future (Le Quéré et al. 2007), although due to uncertainty in observations and in models there is much controversy over predicted trends (Law et al. 2008; Zickfeld et al. 2008; Le Quéré et al. 2008).

As the hydrological cycle is the subject of this research, changes in Southern Ocean salinity characteristics are the focus here, although undoubtedly changes in other characteristics are also important. In terms of changes in salinity of the Southern Ocean, its importance in global climate change has been provided: an increase in stratification in the ACC region could reduce vertical mixing along isopycnals and convective overturning, which in turn could reduce the downward flux of carbon and the upward loss of ocean heat to the atmosphere, resulting in an overall reduction in oceanic uptake of carbon dioxide

(Sarmiento et al. 1998). Freshening of the Southern Ocean can also affect global ocean circulation as it is one of the regions of deep water formation (Aoki et al. 2003). For example, results from simulations using a climate model of intermediate complexity found that enhanced moisture transport from subtropical to subpolar regions in the SH affects the ratios of formation of circumpolar deep water and Antarctic intermediate water, which in turn has the potential to intensify the Atlantic meridional overturning circulation and thus northward oceanic heat transport and air-sea heat exchange (Saenko and Weaver 2003). Additionally, changes in salinity can induce sea level change as a result of firstly the addition and removal of freshwater and secondly the haline contraction factor in sea level calculations (Boyer et al. 2005). Although only the addition of freshwater from continents can lead to a global eustatic rise in sea level, understanding the different contributions to global ocean freshening improves estimates of the observed global sea level change and aids future predictions (Munk 2003).

Changes in stratospheric ozone have already been linked to changes in the Southern Ocean (Toggweiler and Russell 2008; Forster et al. 2010). The positive trend in the SAM during austral summer due to ozone depletion implies an intensification and poleward shift of the surface zonal wind stress and wind stress curl and as these are the driving forces for the ACC and meridional overturning circulation in the Southern Ocean, it follows that ozone depletion has forced changes in the Southern Ocean circulation (Böning et al. 2008; Toggweiler 2009; Forster et al. 2010). Supporting evidence for the poleward shift of the ACC is provided by observations, which show that the southern portion of the Southern Ocean has warmed at the highest rate over last century, suggesting that the temperature gradient associated with the ACC has moved south (Aoki et al. 2003; Gille 2003). Temperature trends in the ACC region have been reproduced in CMIP3 coupled models and

these attribute a large portion of the warming at depth to the increase in surface wind stress (Forster et al. 2010). As the increasing surface wind stress is largely due to stratospheric ozone depletion during austral summer, it can then be inferred that stratospheric ozone depletion is likely to have contributed to the subsurface warming of the ACC and reduced stratification in this region (Forster et al. 2010), which counteracts the increased stratification due to surface warming associated with greenhouse gas forced global warming (Forster et al. 2010). However, the observed increase in freshwater flux during the 20^{th} century increases the stratification of the Southern Ocean and this study attributes this freshening to ozone depletion, as models with ozone depletion have a significantly stronger increasing trend in P–E in high latitudes in austral summer compared to models without ozone depletion. Thus it appears that ozone forcing itself could have competing effects on Southern Ocean stratification.

Obtaining a quantitative estimate of the effect of the increased P–E over the ACC is beyond the scope of this research and additionally is inherently limited by the reliability of precipitation modelling in climate models. Thus it is merely possible to comment briefly on some superficial aspects. That observations during the 20^{th} century show surface freshening over the extent of the ACC (Böning et al. 2008) and surface salinity increases over the SH subtropics (Boyer et al. 2005) is consistent with an increasing trend in P–E in high latitudes and decreasing trend in P–E in mid-latitudes, attributes these changes, at least in part to ozone depletion: the strongest trends in P–E are found in austral summer in models that prescribed ozone forcing. Based on this, stratospheric ozone depletion is likely to have increased surface stratification in the region of the ACC during the 20^{th} century. Following this reasoning, the multimodel-mean for models with ozone recovery in the 21^{st} century predicts weaker trends in P–E compared to models without ozone recovery, so

the stratification due to freshening attributed to ozone forcing in the 20^{th} century may be reversed in the 21^{st} century.

5.3 Future work

To gain a more comprehensive understanding of the influence of stratospheric ozone changes on SH hydrological climate change it is recommended that the sensitivity of results to the methodology used here be investigated. To improve the understanding of how inter-model differences have affected results, the sensitivity of results to the particular models used in the study could be assessed by using different groups of models. Additionally, to remove some uncertainty due to noise and aid more clear conclusions, results could be re-calculated using a 4° latitude by 4° longitude standard grid.

To gain a better understanding into the dynamical mechanisms governing changes in precipitation, further work examining surface wind, temperature and mean sea level pressure changes are recommended, as they could reveal different aspects of extreme weather changes in association with stratospheric ozone depletion and recovery. Particularly, it is recommended the influence of stratospheric ozone on the extratropical westerly jet be investigated on a model-by-model basis, with model bias in jet location and intensity and their corresponding storm track location and intensity examined. Observational data could also be used to improve physical understanding by correlating interannual peaks in ozone concentration and precipitation and investigating cause and effect mechanisms.

Sensitivity studies looking into the differences amongst models in their precipitation-evaporation processes (such as clouds and aerosol number density and sizes) may also be useful. Such studies could provide information about the impacts of stratospheric ozone

depletion and recovery in terms of radiation modification (absorption and scattering) and nucleation that leads to precipitation, influencing both frequency and intensity.

The findings of this study are based solely on multimodel averaging and thus should be treated with care. Although multimodel averaging can reduce model biases, it does not allow direct attribution of SH climate changes to Antarctic stratospheric ozone depletion and recovery. This approach may also underestimate hydrological responses to ozone forcings by averaging models with realistic climatologies and trends with those without them. To better understand the impact of stratospheric ozone depletion and recovery on SH climate, more quantitative studies using climate model sensitivity tests (e.g. McLandress et al. 2011; Polvani et al. 2011) are needed for better quantifying ozone-induced hydrological climate changes in the SH.

Appendix

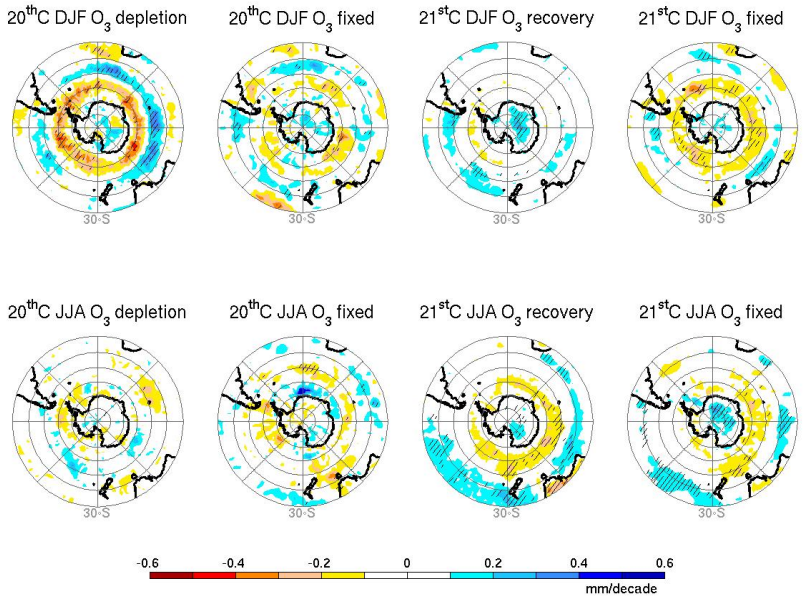

Figure A.1: Multimodel-mean trends in the accumulation of daily precipitation events for the 0.1–1 mm day^{-1} regime for the four model groups. Note that the colour scale is enhanced by a factor of 10 in comparison to Figure 4.14B to allow trends in the accumulation due to very light precipitation to be discerned.

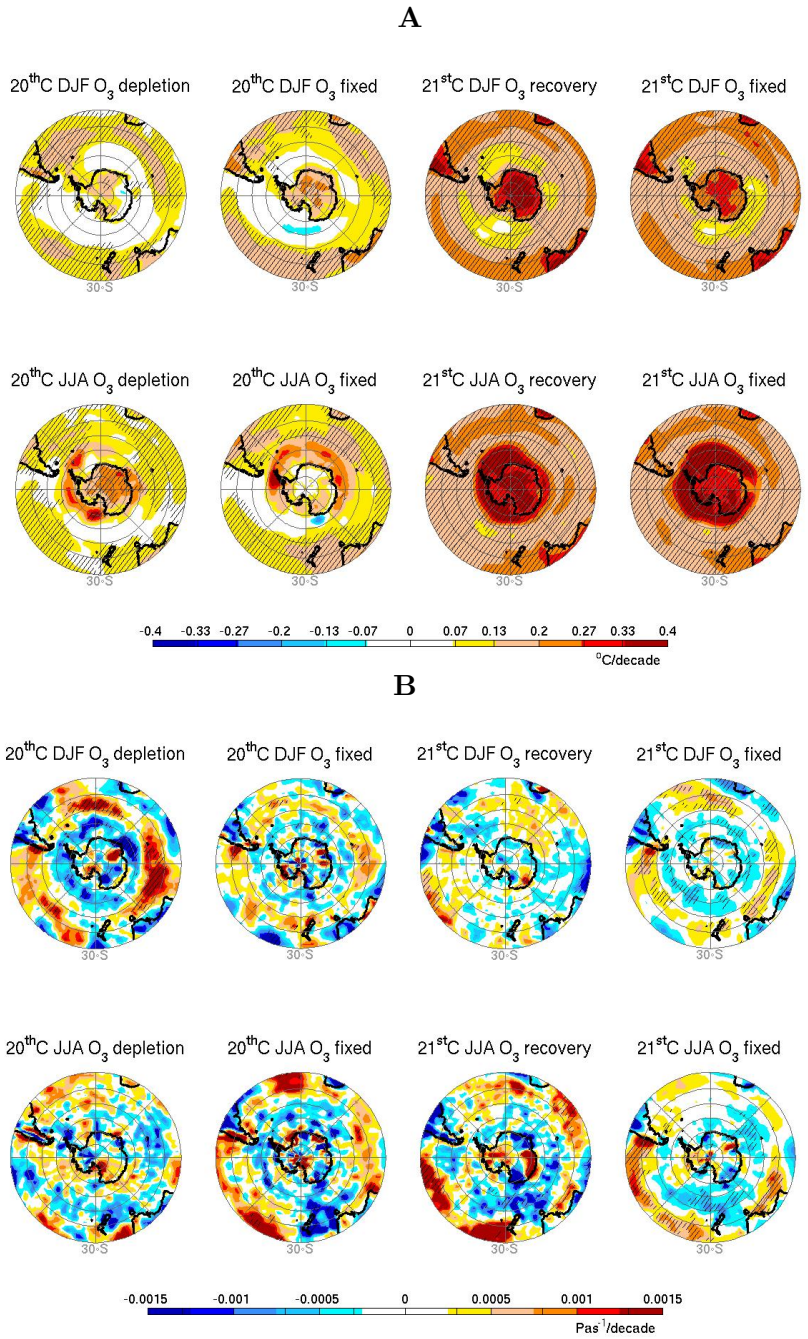

Figure A.2: Multimodel-mean trends in **A** surface air temperature and **B** 500 hPa vertical motion (omega) for the four model groups.

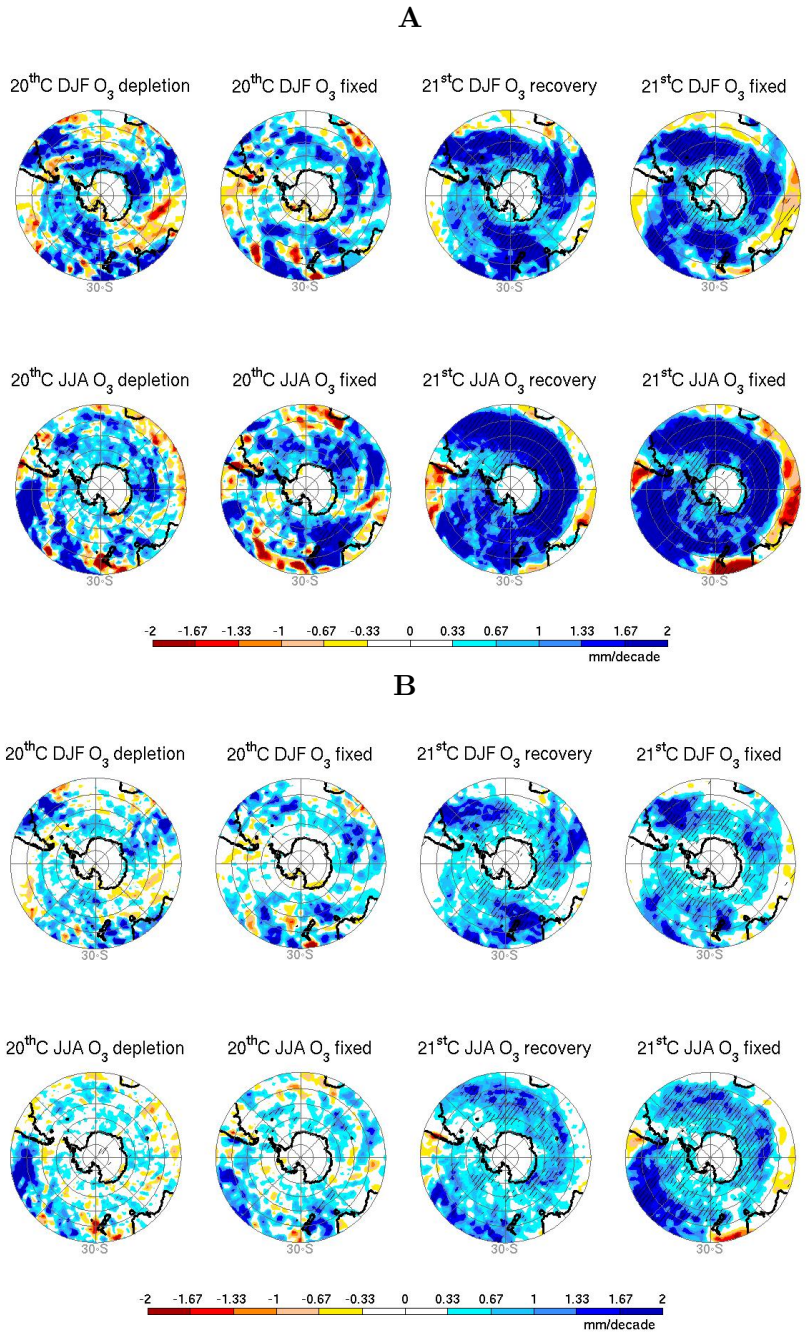

Figure A.3: Multimodel-mean trends in the sum of precipitation exceeding high percentiles. **A** shows 95^{th} percentile and **B** shows 99^{th} percentile for the four model groups.

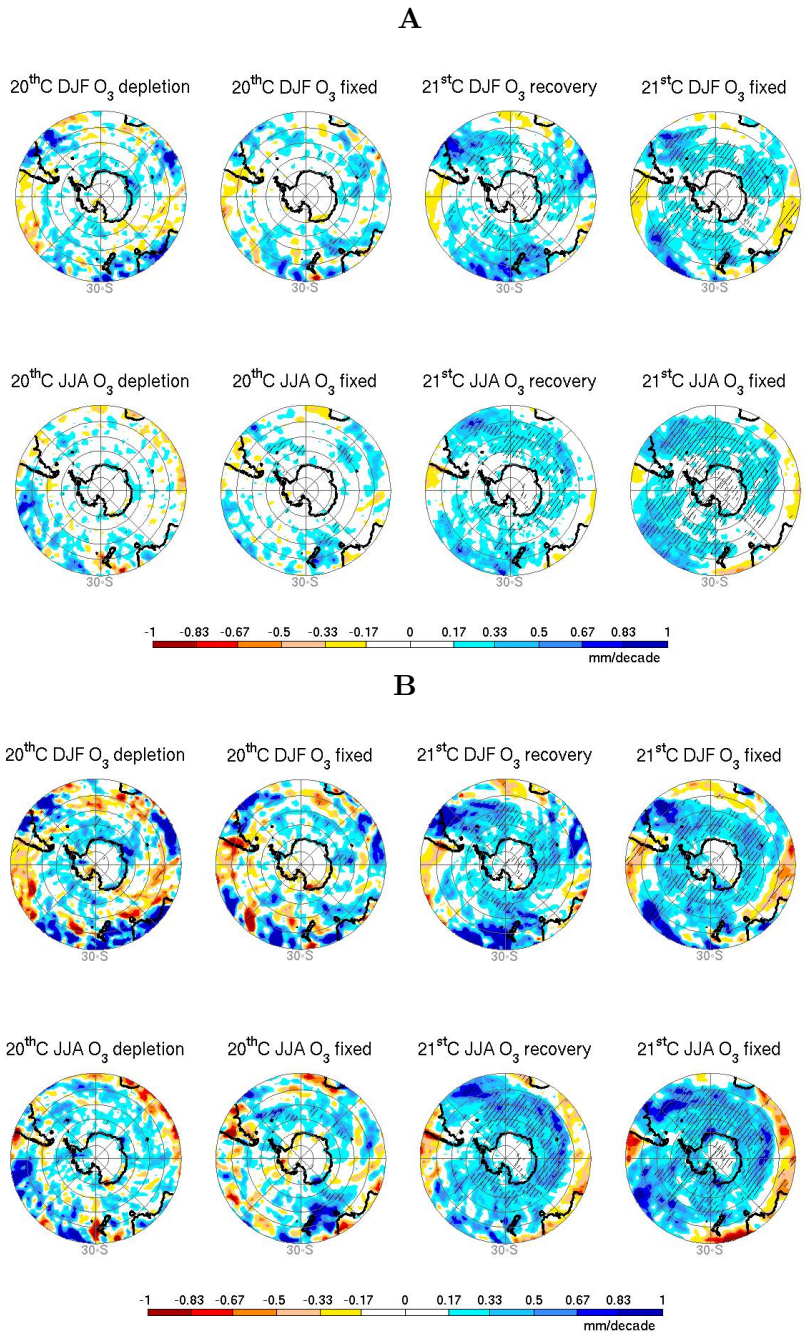

Figure A.4: Multimodel-mean trends in maximum daily precipitation indices. **A** shows maximum one-day precipitation and **B** shows maximum five-day consecutive precipitation) for the four model groups.

References

Adler, R., et al., 2003: The Version-2 Global Precipitation Climatology Project (GPCP) monthly precipitation analysis (1979–present). *Journal of Hydrometeorology*, **4**, 1147–1167.

Aoki, S., M. Yoritaka, and A. Masuyama, 2003: Multidecadal warming of subsurface temperature in the Indian sector of the Southern Ocean. *Journal of Geophysical Research*, **108**.

Arblaster, J. and G. Meehl, 2006: Contributions of external forcings to Southern Annular Mode trends. *Journal of Climate*, **19**, 2896–2905.

Austin, J., et al., 2010: Decline and recovery of total column ozone using a multimodel time series analysis. *Journal of Geophysical Research*, **115**, D00M10.

Barnes, E. and D. Hartmann, 2010: Testing a theory for the effect of latitude on the persistence of eddy-driven jets using CMIP3 simulations. *Geophysical Research Letters*, **37**, L15801.

Bartholy, J. and R. Pongrácz, 2010: Analysis of precipitation conditions for the Carpathian Basin based on extreme indices in the 20th century and climate simulations for 2050 and 2100. *Physics and Chemistry of the Earth*, **35**, 43–51.

Bengtsson, L. and K. Hodges, 2006: Storm tracks and climate change. *Journal of Climate*, **19**, 3518–3543.

Bodeker, G., H. Shiona, and H. Eskes, 2005: Indicators of Antarctic ozone depletion. *Atmospheric Chemistry and Physics*, **5**, 2603–2615.

Böning, C., A. Dispert, M. Visbeck, S. Rintoul, and F. Schwarzkopf, 2008: The response of the Antarctic Circumpolar Current to recent climate change. *Nature Geoscience*, **1**, 864–869.

Boyer, T., S. Levitus, J. Antonov, R. Locarnini, and H. Garcia, 2005: Linear trends in salinity for the World Ocean, 1955–1998. *Geophysical Research Letters*, **32**, L01604.

Brandon, M., 2010: Descriptive physical oceanography: Oceanic density and pressure. Available online from: `http://science.jrank.org/pages/47912/oceanic-density-pressure.html`.

Cai, W. and T. Cowan, 2007: Trends in Southern Hemisphere circulation in IPCC AR4 models over 1950–99: Ozone depletion versus greenhouse forcing. *Journal of Climate*, **20**, 681–693.

Dai, A., 2006: Precipitation characteristics in eighteen coupled climate models. *Journal of Climate*, **19**, 4605–4630.

Dore, M., 2005: Climate change and changes in global precipitation patterns: What do we know? *Environment International*, **31**, 1167–1181.

Emori, S. and S. Brown, 2005: Dynamic and thermodynamic changes in mean and extreme precipitation under changed climate. *Geophysical Research Letters*, **32**, L17706.

ETCCDI, 2009: Climate change indices: Definitions of the 27 core indices. Available online from: `http://cccma.seos.uvic.ca/ETCCDMI`.

Fogt, R., J. Perlwitz, A. Monaghan, D. Bromwich, J. Jones, and G. Marshall, 2009: Historical SAM variability. Part II: Twentieth-century variability and trends from reconstructions, observations, and the IPCC AR4 models. *Journal of Climate*, **22**, 5346–5365.

Forster, P., et al., 2010: Chapter 4: Stratospheric Changes and Climate; in Scientific Assessment of Ozone Depletion: 2010. Global Ozone Research and Monitoring Project 52, World Meteorological Organization.

Fyfe, J., 2003: Extratropical Southern Hemisphere cyclones: Harbingers of climate change. *Journal of Climate*, **16**, 2802–2805.

Gastineau, G. and B. Soden, 2009: Model projected changes of extreme wind events in response to global warming. *Geophysical Research Letters*, **36**, L10810.

Gille, S., 2002: Warming of the Southern Ocean Since the 1950s. *Science*, **295**, 1275–1277.

Gille, S., 2003: Float observations of the Southern Ocean. Part I: Estimating mean fields, bottom velocities, and topographic steering. *Journal of Physical Oceanography*, **33**, 1167–1181.

Gillett, N., T. Kell, and P. Jones, 2006: Regional climate impacts of the Southern Annular Mode. *Geophysical Research Letters*, **33**, L23704.

Gillett, N. and D. Thompson, 2003: Simulation of recent Southern Hemisphere climate change. *Science*, **302**, 273–275.

Gordon, H., S. O'Farrell, M. Collier, M. Dix, L. R. an E. Kowalczyk, T. Hirst, and I. Watterson, 2010: The CSIRO Mk3.5 Climate Model. CAWCR Technical Report 021, The Centre for Australian Weather and Climate Research.

Held, I. and B. Soden, 2006: Robust responses of the hydrological cycle to global warming. *Journal of Climate*, **19**, 5686–5699.

Hendon, H., D. Thompson, and M. Wheeler, 2007: Australian rainfall and surface temperature variations associated with the Southern Hemisphere annular mode. *Journal of Climate*, **20**, 2452–2467.

Jacobs, S., 2006: Observations of change in the Southern Ocean. *Philosophical Transactions of The Royal Society A*, **364**, 1657–1681.

Johanson, C. and Q. Fu, 2009: Hadley cell widening: Model simulations versus observations. *Journal of Climate*, **22**, 2713–2725.

Karpechko, A., N. Gillett, G. Marshall, and A. Scaife, 2008: Stratospheric influence on circulation changes in the Southern Hemisphere troposphere in coupled climate models. *Geophysical Research Letters*, **35**, L20806.

Kharin, V., F. Zwiers, X. Zhang, and G. Hegerl, 2007: Changes in temperature and precipitation extremes in the IPCC ensemble of global coupled model simulations. *Journal of Climate*, **20**, 1419–1444.

Kidston, J. and E. Gerber, 2010: Intermodel variability of the poleward shift of the austral jet stream in the CMIP3 integrations linked to biases in 20th century climatology. *Geophysical Research Letters*, **37**, L09708.

Lambert, S. and J. Fyfe, 2006: Changes in winter cyclone frequencies and strengths simulated in enhanced greenhouse warming experiments: Results from the models participating in the IPCC diagnostic exercise. *Climate Dynamics*, **26**, 713–728.

Law, R., R. Matear, and R. Francey, 2008: Comment on "Saturation of the Southern Ocean CO_2 sink due to recent climate change". *Science*, **319**, 570a.

Le Quéré, C., et al., 2007: Saturation of the Southern Ocean CO_2 sink due to recent climate change. *Science*, **316**, 1735–1738.

Le Quéré, C., et al., 2008: Response to Comments on "Saturation of the Southern Ocean CO_2 sink due to recent climate change". *Science*, **319**, 570c.

Levitus, S., J. Antonov, and T. Boyer, 2005: Warming of the World Ocean, 1955–2003. *Geophysical Research Letters*, **32**, L02604.

Mailhot, A., A. Kingumbi, G. Talbot, and A. Poulin, 2010: Future changes in intensity and seasonal pattern of occurrence of daily and multi-day annual maximum precipitation over Canada. *Journal of Hydrology*, **388**, 173–185.

Marshall, G., 2003: Trends in the Southern Annular Mode from observations and reanalyses. *Journal of Climate*, **16**, 4134–4143.

McLandress, C., T. Shepherd, J. Scinocca, D. Plummer, M. Sigmond, A. Jonsson, and M. Reader, 2011: Separating the dynamical effects of climate change and ozone depletion: Part 2. Southern Hemisphere troposphere. *Journal of Climate*, **24**, 1850–1868.

Meehl, G., J. Arblaster, and C. Tebaldi, 2005: Understanding future patterns of increased precipitation intensity in climate model simulations. *Geophysical Research Letters*, **32**, L18719.

Min, S.-K., X. Zhange, F. Zwiers, and G. Hergerl, 2011: Human contribution to more-intense precipitation extremes. *Nature*, **470**, 378–381.

Morgenstern, O., P. Braesicke, M. Hurwitz, and F. O'Connor, 2008: The world avoided by the Montreal Protocol. *Geophysical Research Letters*, **35**, L16811.

Munk, W., 2003: Ocean freshening, sea level rising. *Science*, **300**, 2041–2043.

NOAA/OAR/ESRL PSD, 2010a: NCEP reanalysis derived data. Available online from: `http://www.esrl.noaa.gov/psd/`.

NOAA/OAR/ESRL PSD, 2010b: NOAA extended reconstructed sea surface temperature V3b data. Available online from: `http://www.esrl.noaa.gov/psd/`.

O'Gorman, P. and T. Schneider, 2009: The physical basis for increases in precipitation extremes in simulations of 21st-century climate change. *PNAS*, **106**, 14 773–14 777.

Pal, I. and A. Al-Tabbaa, 2009: Trends in seasonal precipitation extremes - An indicator of 'climate change' in Kerala, India. *Journal of Hydrology*, **367**, 62–69.

Pawlowicz, R., 2005: M-Map: A mapping package for Matlab. Available online from: `http://www.eos.ubc.ca/ rich/map.html`.

Perlwitz, J., S. Pawson, R. Fogt, J. Nielson, and W. Neff, 2008: Impact of stratospheric ozone hole recovery on Antarctic climate. *Geophysical Research Letters*, **35**, L08714.

Peterson, T., C. Folland, G. Gruza, W. Hogg, A. Mokssit, and N. Plummer, 2001: Report on the activities of the Working Group on Climate Change Detection and Related Rapporteurs 1998-2001. Tech. Rep. WCDMP-47, WMO-TD 1071, World Meteorological Organization.

Polvani, L., D. Waugh, G. Correa, and S.-W. Son., 2011: Stratospheric ozone depletion: The main driver of 20th century atmospheric changes in the Southern Hemisphere. *Journal of Climate*, **24**, 795–812.

Randall, D., et al., 2007: Climate models and their evaluation; in Climate Change 2007: The Physical Sciences Basis. Contribution of Working Group I to the Fourth Assessment Report of the Intergovernmental Panel on Climate Change. Tech. rep., Intergovernmental Panel on Climate Change. Edited by S. Solomon et al.

Saenko, O. and A. Weaver, 2003: Atlantic deep circulation controlled by freshening in the Southern Ocean. *Geophysical Research Letters*, **30**.

Sarmiento, J., T. Hughes, R. Stouffer, and S. Manabe, 1998: Simulated resoponse of the ocean carbon cycle to anthropogenic climate warming. *Nature*, **393**, 245–249.

Scoccimarro, E., S. Gualdi, P. Fogli, E. Manzini, A. Grezio, and A. Navarra, 2007: INGV - SXG: A Coupled Atmosphere Ocean Sea-Ice General Circulation Climate Model. Tech. rep., Centro Euro-Mediterraneo per i Cambiamenti Climatici.

Seidel, D., Q. Fu, W. Randall, and T. Reichler, 2008: Widening of the tropical belt in a changing climate. *Nature Geoscience*, **1**, 21–24.

Shindell, D. and G. Schmidt, 2004: Southern Hemisphere climate responses to ozone changes and greenhouse has increases. *Geophysical Research Letters*, **31**, L18209.

Solomon, S., D. Qin, M. Manning, Z. Chen, M. Marquis, K. Averyt, M. Tignor, and H. Miller (eds.), 2007: Contribution of Working Group I to the Fourth Assessment Report of the Intergovernmental Panel on Climate Change. Tech. rep., Intergovernmental Panel on Climate Change.

Son, S.-W., N. Tandon, M. Lorenzo, and D. Waugh, 2009: Ozone hole and Southern Hemisphere climate change. *Geophysical Research Letters*, **36**, L15705.

Son, S.-W., et al., 2008: The impact of stratospheric ozone recovery on the Southern Hemisphere westerly jet. *Science*, **320**, 1486–1489.

Son, S.-W., et al., 2010: Impact of stratospheric ozone on Southern Hemisphere circulation change: A multimodel assessment. *Journal of Geophysical Research*, **115**, D00M07.

Sun, Y., S. Solomon, A. Dai, and R. Portmann, 2007: How often will it rain? *Journal of Climate*, **20**, 4801–4818.

Thompson, D. and S. Solomon, 2002: Interpretation of recent Southern Hemisphere climate change. *Science*, **296**, 895–899.

Thompson, D. and J. Wallace, 2000: Annular modes in the extratropical circulation. Part I: Month-to-month variability. *Journal of Climate*, **13**, 1000–1016.

Toggweiler, J., 2009: Shifting Westerlies. *Science*, **323**, 1434–1435.

Toggweiler, J. and J. Russell, 2008: Ocean circulation in a warming climate. *Nature*, **451**, 286–288.

Ummenhoffer, C., A. Gupta, and M. England, 2009: Causes of late twentieth-century trends in New Zealand precipitation. *Journal of Climate*, **22**, 3–19.

WCRP CMIP3, 2010: WCRP CMIP3 multi-model database. Available online from: `ftp://ftp-esg.ucllnl.org/`.

WHOI OAFlux Project, 2009: OAFlux global ocean evaporation data. Available online from: `http://oaflux.whoi.edu/evap.html`.

Wong, A., N. Bindoff, and J. Church, 1999: Large-scale freshening of intermediate waters in the Pacific and Indian oceans. *Nature*, **400**, 440–443.

Yu, L., X. Jin, and R. Weller, 2008: Multidecade Global Flux Datasets from the Objectively Analyzed Air-sea Fluxes (OAFlux) Project: Latent and Sensible Heat Fluxes, Ocean Evaporation, and Related Surface Meteorological Variables. OAFlux Project Technical Report OA-2008-01, Woods Hole Oceanographic Institution.

Zickfeld, K., J. Fyfe, M. Eby, and A. Weaver, 2008: Comment on "Saturation of the Southern Ocean CO_2 sink due to recent climate change". *Science*, **319**, 570b.